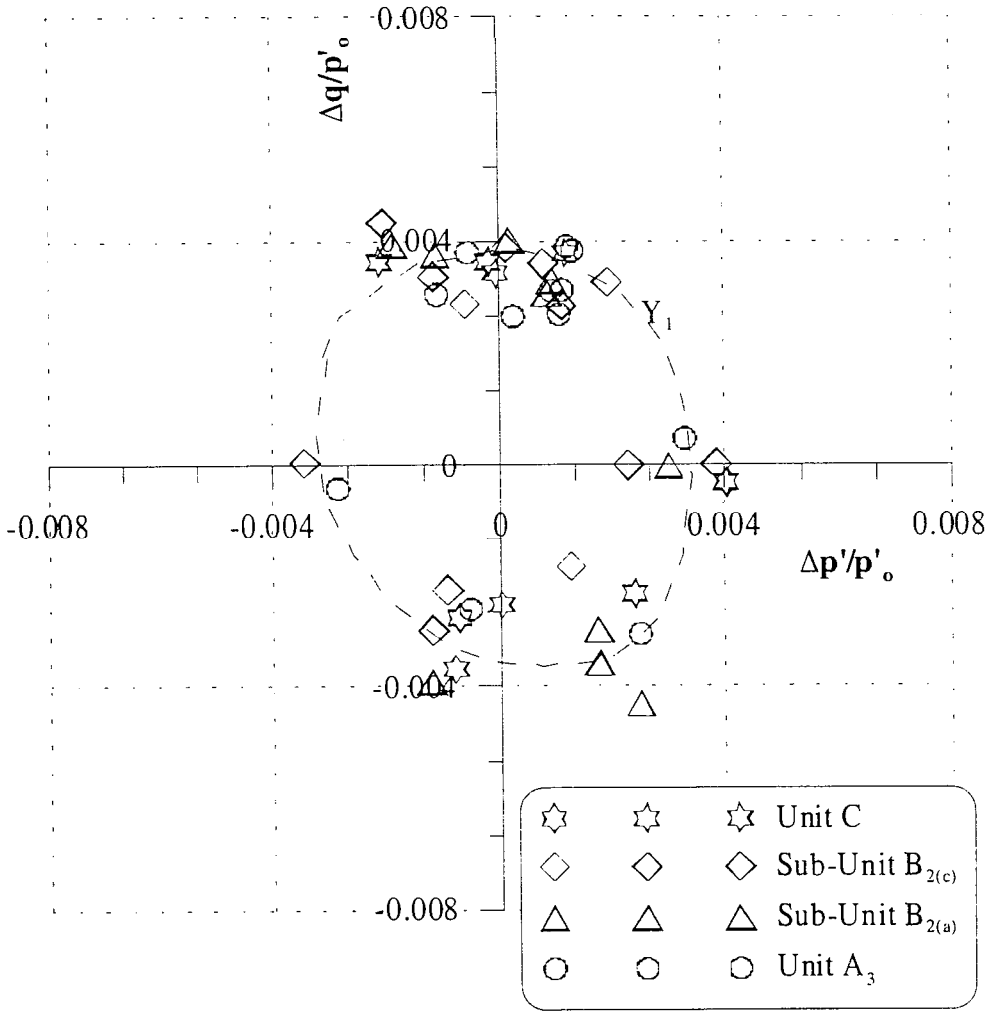

Figure 8.83: Normalised Y_1 yield locus for different lithological units

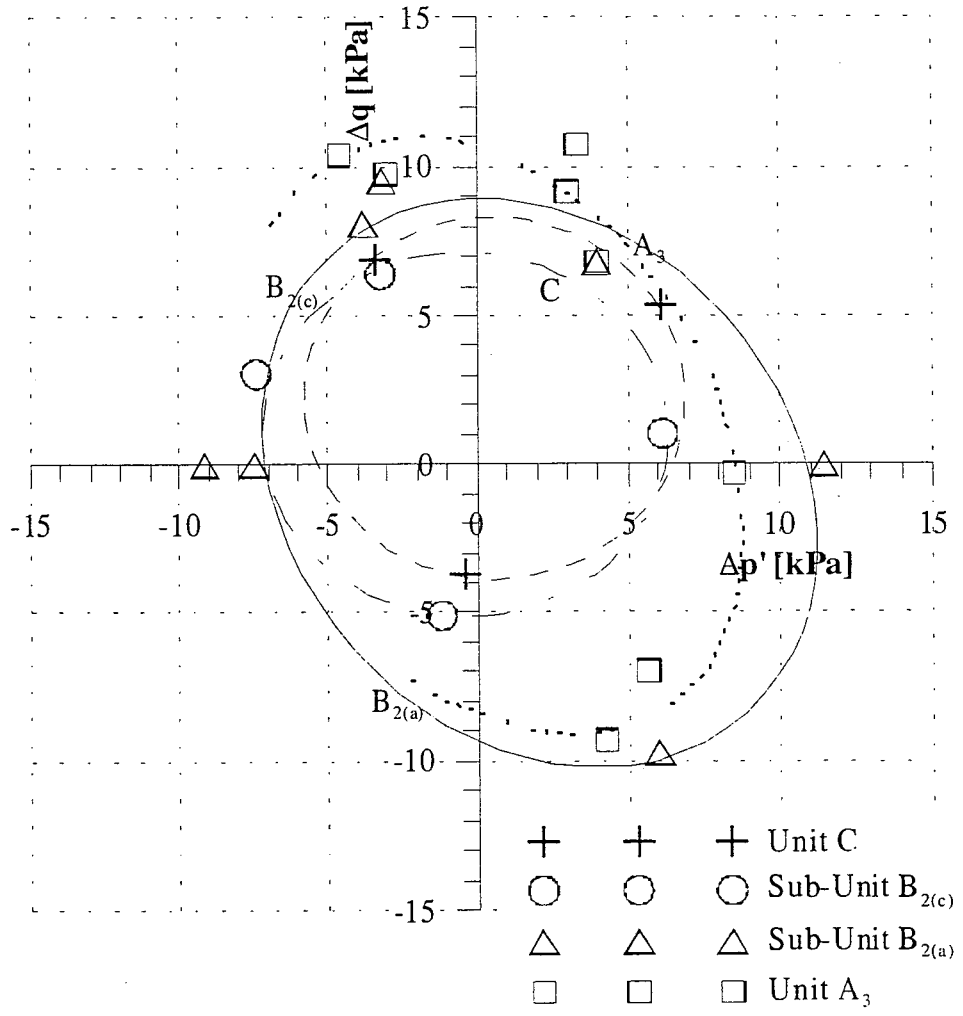

Figure 8.84: Y_2 yield locus for different lithological units

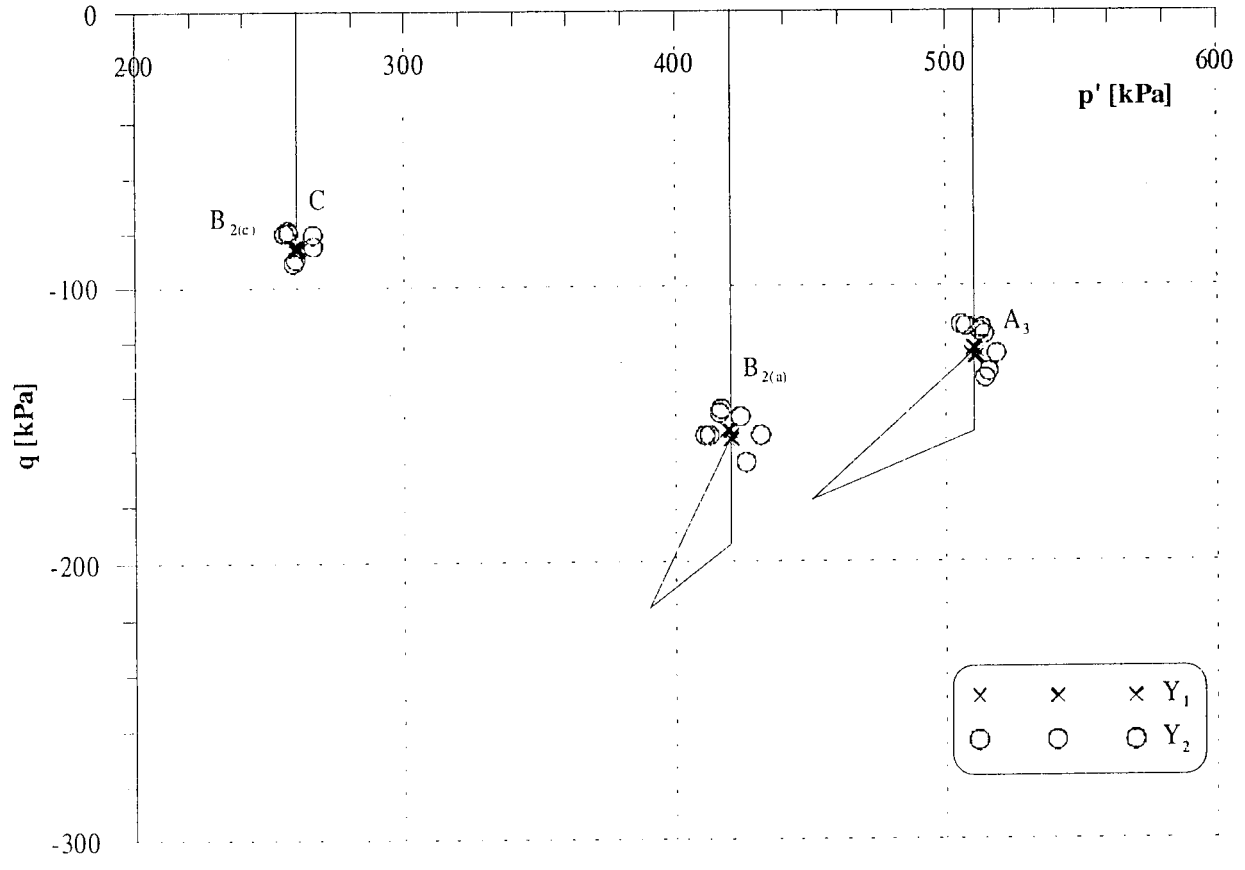

Figure 8.85: Contours of the kinematic regions and approach stress paths for different lithological units

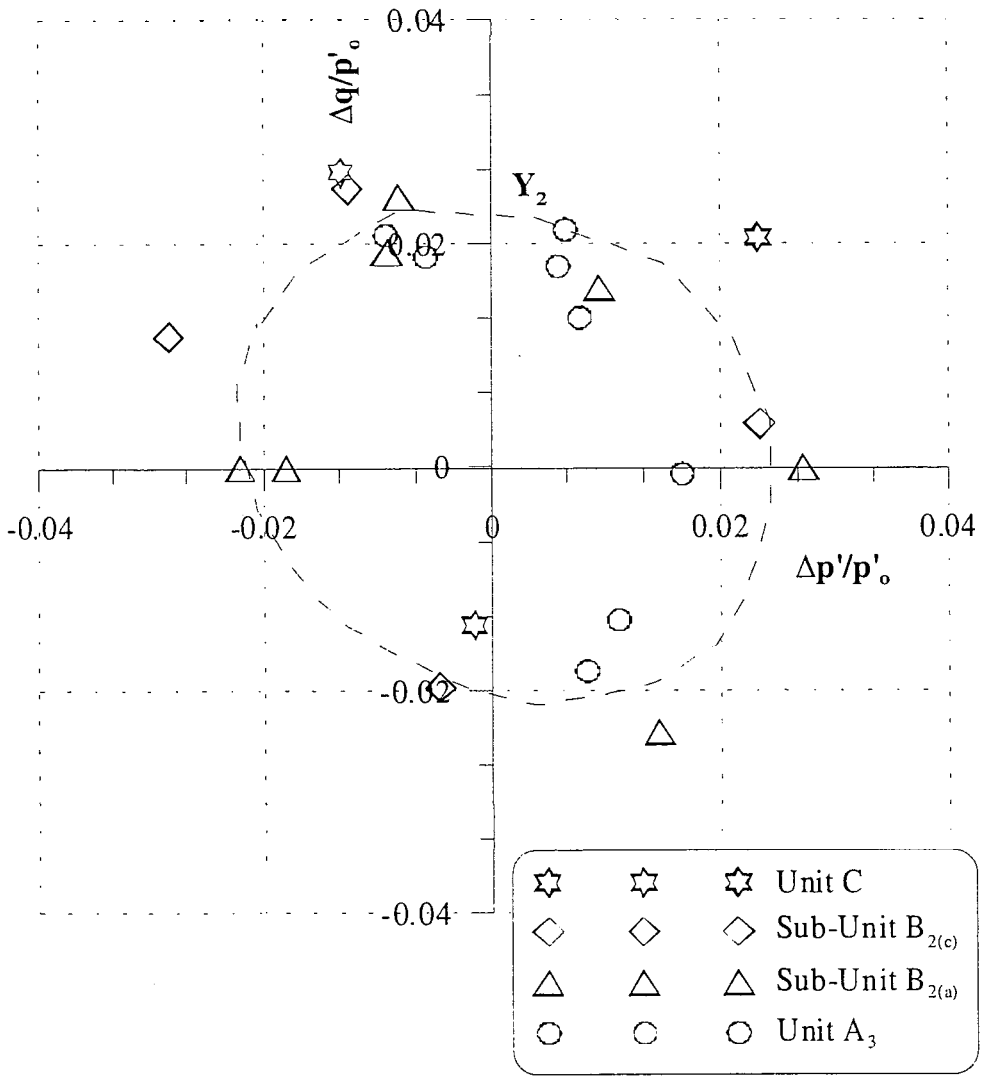

Figure 8.86: Normalised Y_2 yield locus for samples from different lithological units

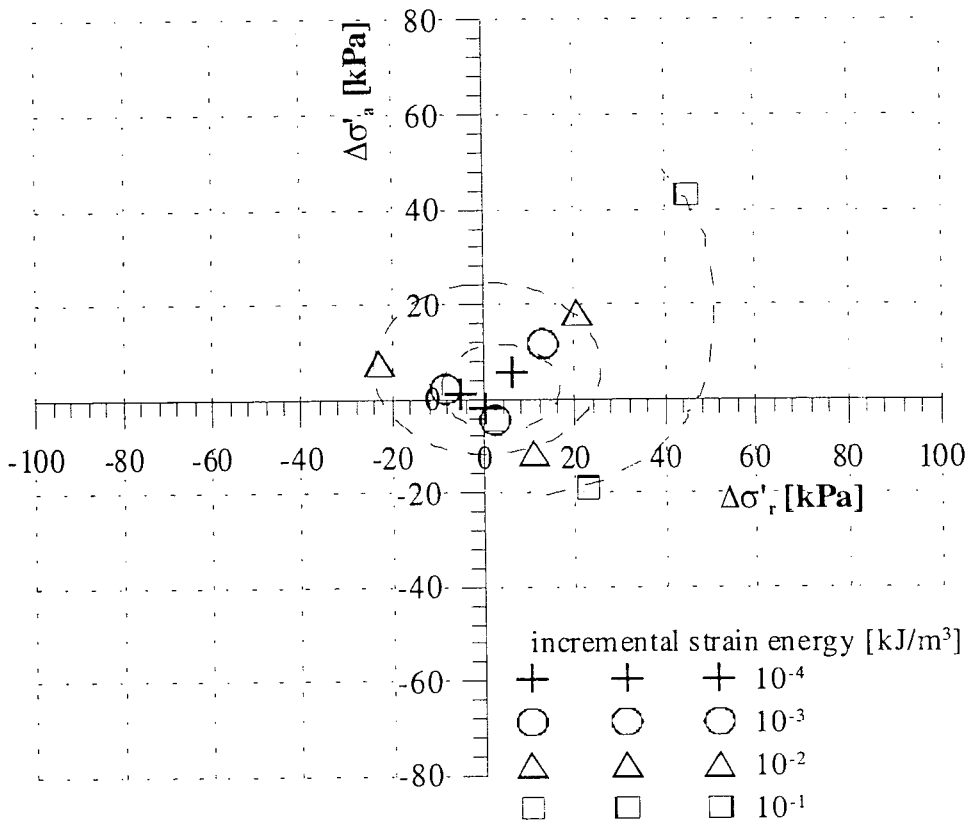

Figure 8.87: Contours of different incremental strain energies for samples from Unit C

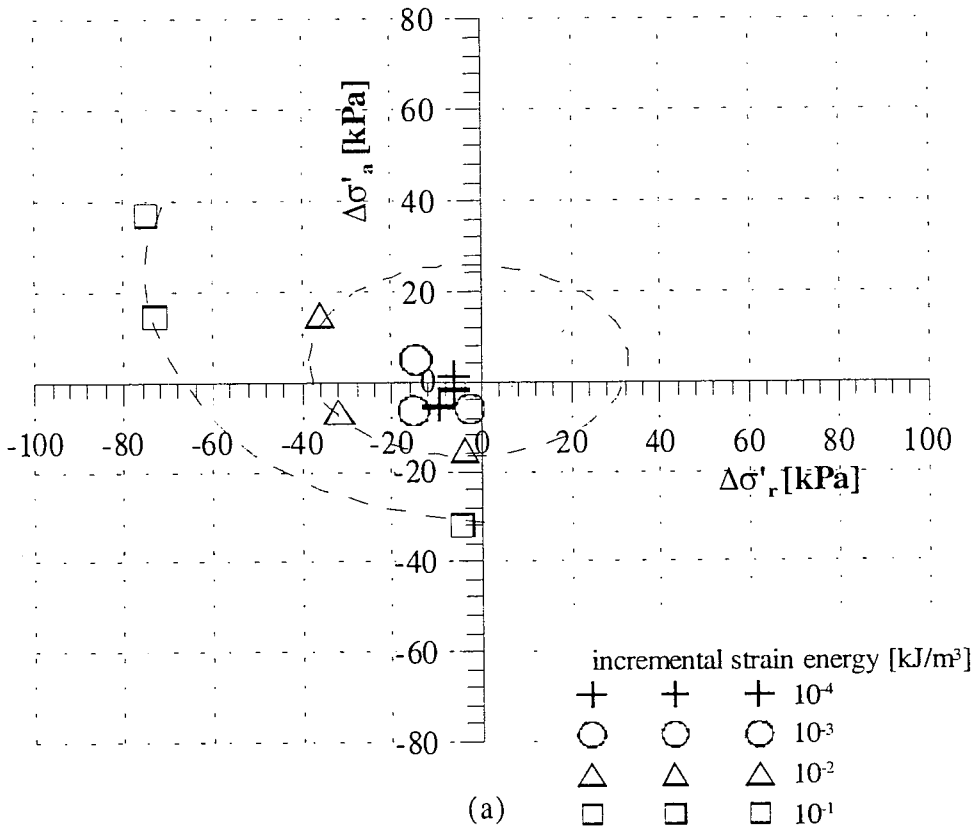

(a)

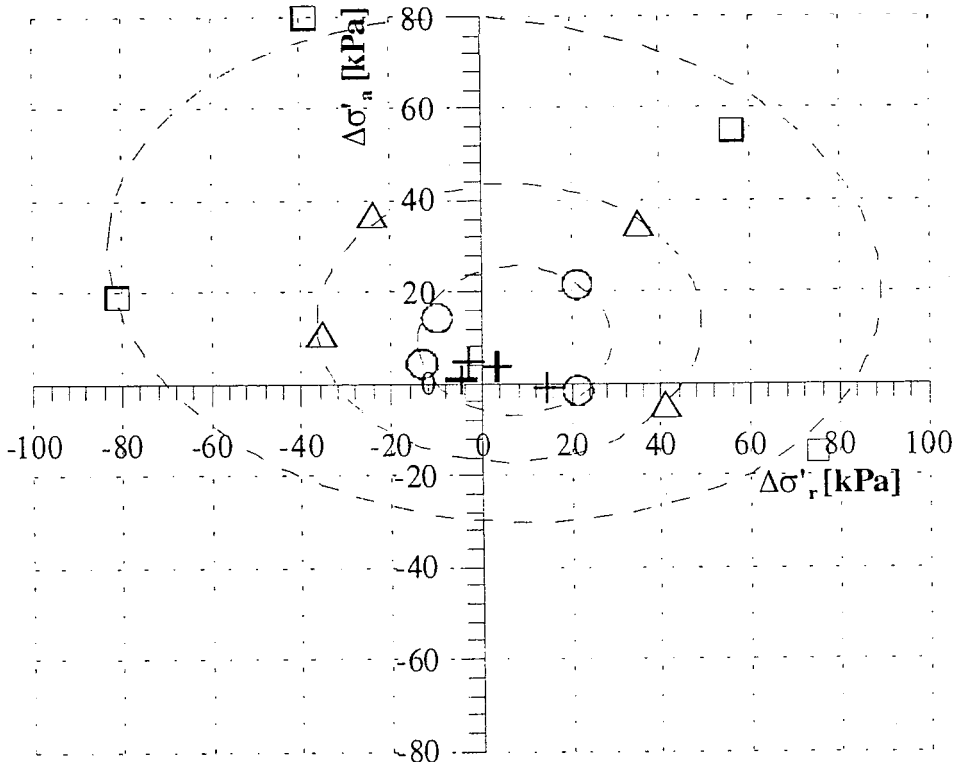

(b)

Figure 8.88: Contours of different incremental strain energies for samples from Unit $B_{2\,(a)}$ Sub-Unit $B_{2(c)}$ (b) Sub-Unit $B_{2(a)}$

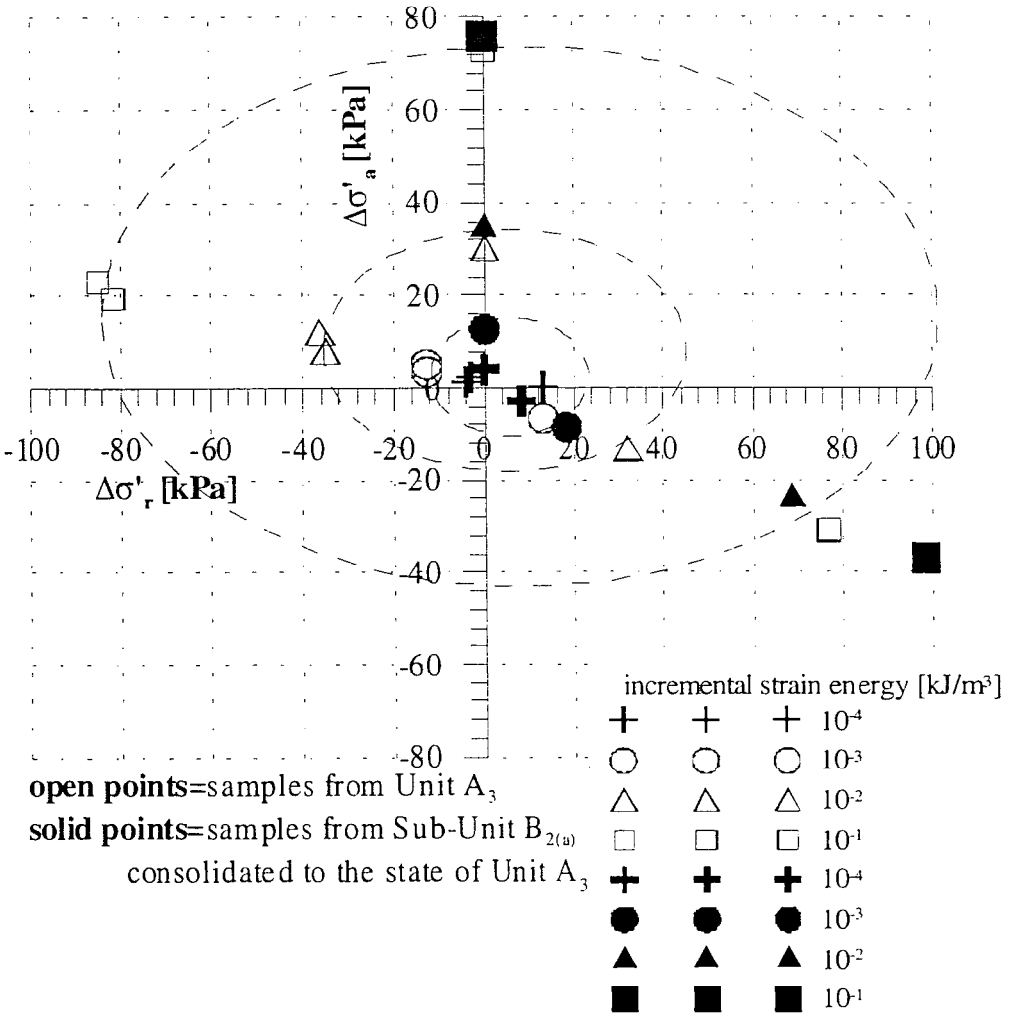

Figure 8.89: Contours of different incremental strain energies for samples from Unit A_3 and from Sub-Unit $B_{2(a)}$ consolidated to the in situ stress state of Unit A_3

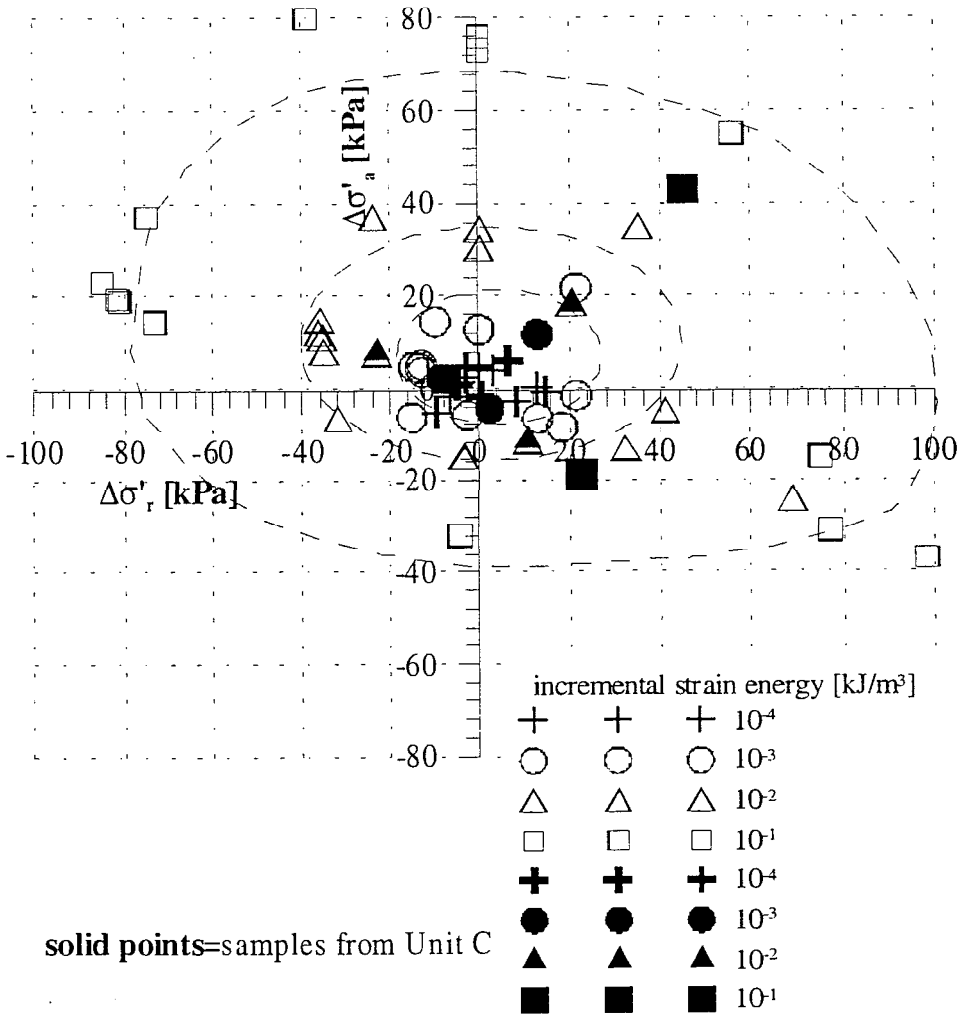

Figure 8.90: Contours of different incremental strain energies for samples from different lithological units

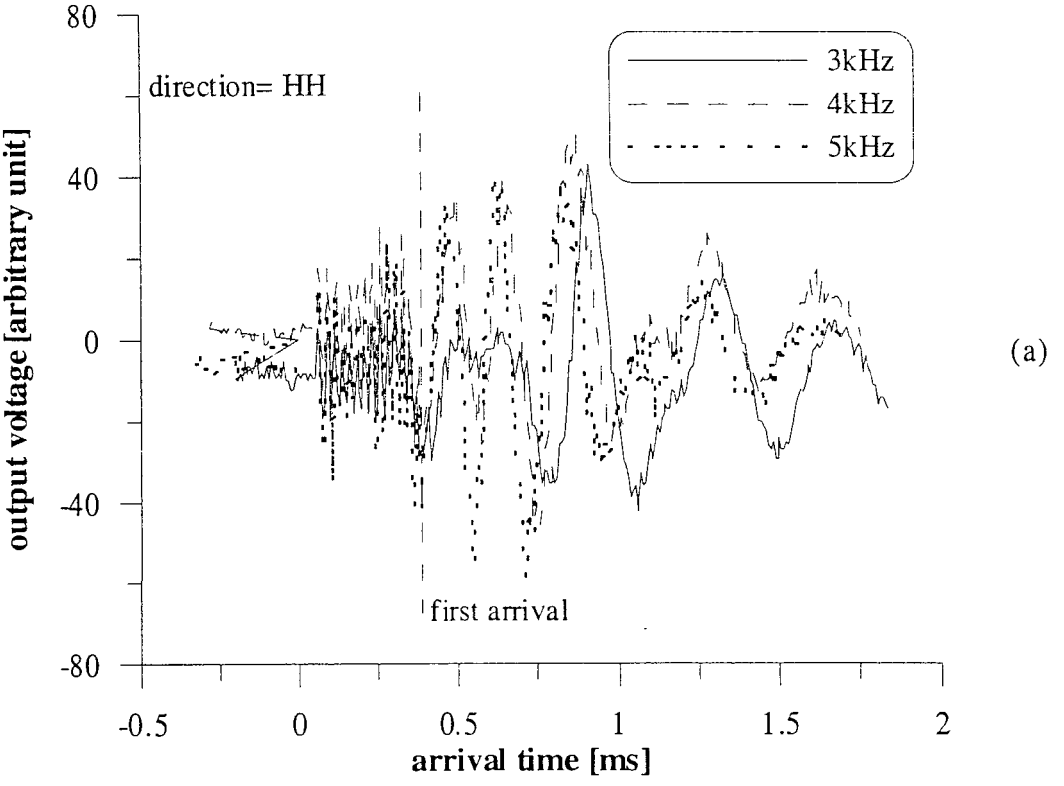

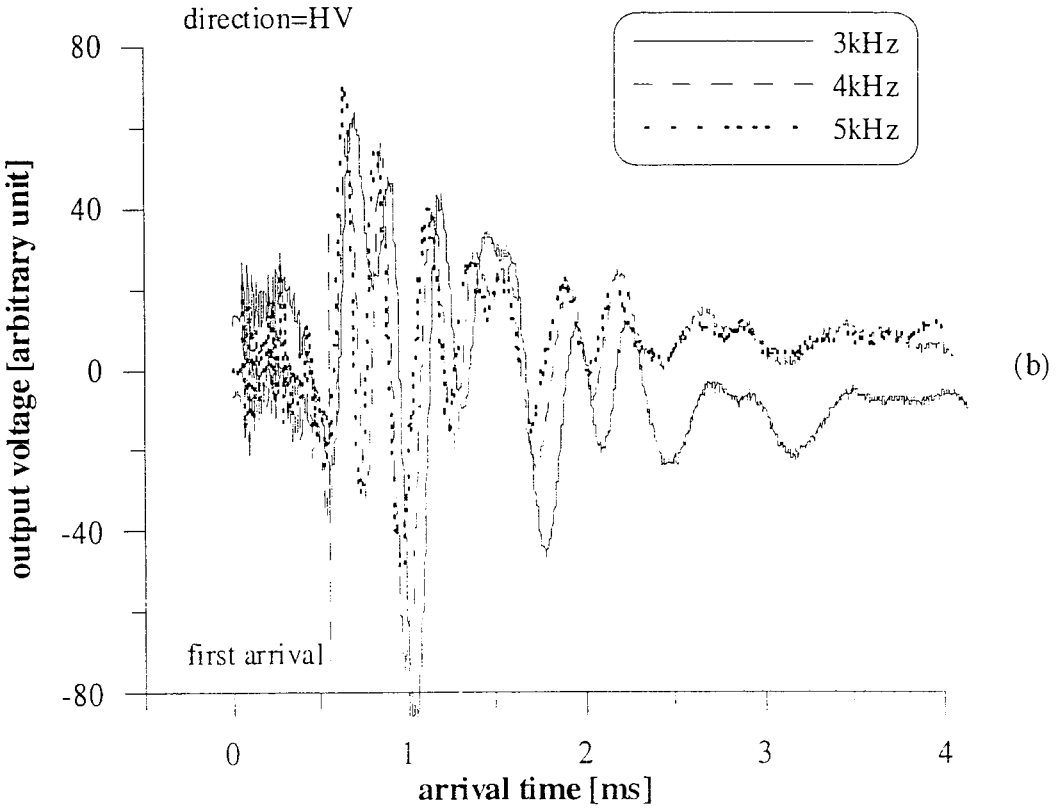

Figure 8.91: Bender element signal through a sheared sample (a) horizontal polarisation and horizontal propagation (b) vertical polarisation and horizontal propagation

9 EFFECTS OF RECENT STRESS HISTORY

9.1 Introduction

In this chapter, the influence of recent stress history on the behaviour of the clay will be discussed on the basis of the results of the tests on Samples 17SH and 17.3SH. The test procedures for these samples were described in detail in Section 5.3.5. The samples were consolidated to their equivalent isotropic in situ stress state and subjected to a set of stress path rotations and undrained probes. One of the samples tested started from a slightly anisotropic state of q=-10kPa. This deviatoric stress, though, was sufficiently small to consider the stress state nearly isotropic. Starting from an isotropic state was a necessary choice to avoid interacting effects due to the vicinity of the failure lines in extension or compression, which might induce a softer response and obscure the effect of recent stress history (see Section 2.5.2).

In the tests, the influences of three main factors were considered, which are the angle of rotation between the outgoing path and the approach stress path, the length of the approach stress path and the creep rates before probing. The analysis of the results will be conducted focussing on the strains involved. Only angles of rotation of 0° and 180° were supposed to be used in the probes because, from the literature, these angles were expected to give the more distinguishable results. However, the effective angles of rotation were different from the nominal values of 0° and 180° because the probes were undrained. Two cases were considered, which had different lengths of the approach stress path. In the first case, the samples were subjected to a small approach stress path that coincided approximately with the dimension of the Y_2 surface for this depth. They were then subjected to undrained shear probes either directly after reaching the initial stress state or after the creep had reduced to negligible values. In the second case, the samples were subjected to a long approach stress path of about 100kPa and then to undrained probes after the creep had reduced.

The approach stress paths were conducted at low stress rates to avoid the development of significant excess pore pressures, which was controlled to be lower than 5% of the current effective stress. The rate of loading was further reduced in the proximity of the initial stress state so that it could be reached in a fully drained condition. The shear probes were undrained, stress controlled and, in most cases, were conducted in extension.

9.2 Case 1: short approach stress path

Two sets of tests were conducted with the approach stress path length corresponding to about 10kPa, which is, approximately, the dimension of the Y_2 surface estimated for Sub-unit $B_{2(b)}$. The two sets of tests differed in the rate of creep allowed before starting the shear probes and were conducted on Samples 17SH and 17.3SH. For Sample 17SH, the creep rate was allowed to reduce before probing, while no creep was allowed for Sample 17.3SH.

9.2.1 Creep allowed

The first set of tests was conducted on Sample 17SH consolidated to the stress state of p'=330kPa and q=-10kPa, indicated as Point O in Figure 9.1. From this stress state, the sample was extended at p' constant, to q=-20kPa (Point C in Figure 9.1) and re-compressed back to q=-10kPa at a rate of 1.5kPa/h. The stresses were held at Point O for a few days, until the creep rates had reduced to negligible values and then an undrained extension probe was performed having a 157° rotation from the approach stress path. This stress controlled probe, referred as 17-157°$_e$, was supposed to reach a minimum q of about –30kPa, but problems in the control system caused the control to stop at about –25kPa after which creep developed. This problem, though, did not compromise the probe results. At the end of the probe, the sample was compressed from the Point O in Figure 9.1 to Point B at q=0kPa at constant p' and then brought back to Point O at a rate of 1.5kPa/h. Creep was allowed reduce to negligible values before the new probe in extension was performed having a 23° rotation from the approach stress path. This second probe will be called 17-23°$_e$.

The strains developed by the samples during the approach stress paths for both probes are summarised in Table 9.1 and were of the order of 0.005% for the volumetric strain. The creep rates before probing are shown in Figure 9.2a. The axial strain rates are considered due to the better resolution of the local LVDTs. The values measured of about 10^{-4}%/h, were of the same order of magnitude as the resolution of the local LVDTs. The undrained probes were conducted at a rate of –5kPa/h, corresponding to strain rates of about -0.003%/h (Figure 9.2b), around 30 times faster than the creep strains.

The stress-strain curves for Probes 17-157°$_e$ and the 17-23°$_e$ are shown in Figure 9.3. The data for the two probes seem coincident and cannot be distinguished. Similarly, no difference can be seen in the stiffness degradation curves for the two probes, as shown in Figure 9.4. Not only is the elastic stiffness for the two probes the same, as expected from probes starting from the same stress state, but also the stiffness degradation with strains is the same, regardless the different approach stress paths. There does not seem to be any effect of the recent stress history on the stress-strain and stiffness behaviour for these samples, which had not been strained greatly during the approach stress path and that had been allowed to creep until the creep strains reduced to negligible values.

A set of tests identical to that described above was performed on Sample 17.3SH before conducting the probes described below, obtaining identical results.

9.2.2 Creep not allowed

The probes performed on Sample 17.3SH started from a stress state of p'=330kPa and q=0kPa, which corresponds to the Point A in Figure 9.5. From the state at A, the sample was consolidated at constant p' to a deviatoric stress of q=10kPa, (A' to O' in Figure 9.5) and held at this stress state for three hours before performing an undrained shear probe in compression that had a rotation of about 75° from the direction of the approach stress path and reached a maximum

q of about 37kPa. The creep time of three hours was chosen to be in agreement with the procedures of the tests conducted by Atkinson et al. (1990). After the shear probe, the sample was re-consolidated from O' to B' and back to O' and, after three hours at the Point O', it was sheared undrained in compression with a 105° rotation from the approach stress path. The two shear probes will be named 17.3-75°$_c$ and 17.3-105°$_c$ respectively. The approach stress paths were conducted at stress rates of about 0.5kPa/h, which is lower than the rate used for the set of probes discussed in Section 9.2.1, due to organizational problems with the timing of the probes. The shear probes had to be carried out under observation and, considering that only three hours at constant stresses could be allowed, the approach stress paths had to be performed during the night. As shown below, the use of a slower strain rate for the approach stress path did not affect the results in comparison with the probes described in Section 9.2.1 because in that case the creep rates were allowed to reduce before probing. A condition of full drainage was ensured in both cases.

The strains developed during the approach stress paths are summarised in Table 9.2 and are in the order of 0.015% for the volumetric strain. The creep rates before probing are shown in Figure 9.6, where also the strain rates during the approach stress paths are included. In the three hours when the load was held constant, the creep rates had started to reduce from the rates during loading, but were still about 0.0006%/h when the probes started. The shear probes were stress controlled at a rate of 5kPa/h, which corresponded to strain rates of about 0.003%/h at the beginning of the probes, around five times faster than the creep strain rates. For axial strains larger than 0.004%, the strain rates started to increase, particularly for sample 17.3-75°$_c$, as shown in Figure 9.6b. The stress-strain curves for the two probes in Figure 9.7 show that the response for Probe 17.3-105°$_c$ is stiffer than the response of Probe 17.3-75°$_c$ and this is confirmed by the stiffness degradation curves of the two probes shown in Figure 9.8. The two probes have the same elastic stiffness, but the sample with the lower angle of rotation from the approach stress path has a stiffness that degrades faster.

The recent stress history therefore influences the sample behaviour if the creep is not allowed to reduce, even after an approach stress path that had not produced large strains.

9.3 Case2: long approach stress path

On Sample 17.3SH, two more undrained shear probes were performed in extension after long consolidation stress paths of about 100kPa. The consolidation paths and the probes are shown in Figure 9.9. From the initial stress state of p'=330kPa and q=0kPa the sample was consolidated at constant p' to q=100kPa and back to 0kPa (O"-B"-O" in Figure 9.9). The stresses were held at the Point O" to allow the reduction of the creep strains and then an undrained shear probe in extension was performed, having a 30° rotation from the direction of the approach stress path. After the probe, the sample was re-consolidated at constant p' to the stress state of q=-100kPa and back to q=0kPa (O"-C"-O" in Figure 9.9) and, after creep had reduced to negligible values, subjected to a second undrained probe in extension, having a 150° rotation from the approach stress path. These probes will be named 17.3-L30°$_e$ and 17.3-L150°$_e$, where the "L" refers to the long approach stress path.

The strains developed during the approach stress paths are summarised in Table 9.3 and are of the order of 0.2% for the volumetric strain. The creep rates before probing are shown in Figure 9.10a and were of the order of 10^{-4}%/h, and were virtually not measurable. The probes were stress controlled at a stress rate of –5kPa/h, corresponding to initial strain rates of about -0.003%/h, around 30 times faster than the creep rates. For axial strains higher than 0.004%, the strain rates started to increase, particularly for Sample 17.3-L30°$_e$, as shown in Figure 9.10b. The stress-strain curves for the two probes are shown in Figure 9.11 and clearly demonstrate a stiffer response for Probe 17.3-L150°$_e$ than for Probe 17.3-L30°$_e$. The stiffness degradation curves for the two curves also confirm this result (Figure 9.12), showing that, from the same elastic stiffness, the probe of 30° rotation has a stiffness that degrades faster than that for a probe of 150° rotation. The recent stress history, therefore, seems to influence the clay

behaviour, even when a long time for the creep reduction had been allowed, if the strains developed by the sample during the approach stress path are significant.

From the analyses conducted, there seems to emerge a relationship between the strains developed during the approach stress path and the creep. For a length of the approach stress path that is below the Y_2 region, which corresponds to no large strains being developed in the samples during the approach stress paths, the recent stress history affects the sample behaviour only if no creep is allowed before probing. However, if creep is allowed before probing, then the strains developed during the approach stress path become important. For axial strains rates that are high relative to the creep rate, the effect of the angle of rotation from the previous stress path can only be seen if sufficient strains developed during the approach path. If the sample is not strained sufficiently during the approach stress path, the rest time at the initial state becomes its recent stress history and is able to delete the effects of the angle of rotation. A question then arises about the threshold strains above which the effects of the recent stress history would be seen.

The existence of some conditions that allow the effects of recent stress history to be seen re-opens the debate on the existence of recent stress history effects. The results of the present research are in agreement with both the study conducted by Atkinson et al. (1990) who observed effects of recent stress history and with the tests performed by Clayton & Heymann (2001), who could not see the recent stress history effects, although the writer does not agree with their conclusions. These studies were discussed in Section 2.5.2, but a re-interpretation of those results could be attempted here on the basis of the results of the present research. Atkinson et al. (1990) used a stress rate of 5kPa/h for their consolidation path that was about 90kPa long. Although only the stresses involved were mentioned, this stress path seems sufficient to induce the development of large strains on a reconstituted sample. The authors then allowed three hours of creep before probing because, above that time, they could not measure further strains with the instrumentation they were using. The probes in the present research, conducted with a better resolution instrumentation,

demonstrated that even using lower consolidation rates and a short approach stress path, three hours are not sufficient for the creep strains to reduce to values that do not affect the behaviour of natural London Clay samples. The effects of recent stress history observed by Atkinson et al. (1990), therefore, could be due to the large strains developed during the approach stress path and, possibly, to the combined effect of these strains with residual creep strains.

Clayton & Heymann (2001), instead, were unable to see any effect of recent stress history on Bothkennar clay samples subjected to shear probes having different angles of rotation from an approach stress path of about 9kPa and creep strains that had reduced to negligible values before probing. The stress path they used, though, had comparable dimensions to the Y_2 surface measured on Bothkennar clay (Smith & Jardine, 1992). It is likely that the sample had not been subjected to large strains during the approach stress path and therefore the rest time at the constant stresses before probing became its recent stress history deleting the effects of the previous stress paths.

The examples considered above started from isotropic stress states, which seem to the writer to be more appropriate to investigate the effects of recent stress history. Clayton & Heymann (2001) included in their recent stress history study the results of probes on London Clay samples tested from an initial anisotropic state. They found that the stress path that moved towards the failure line had stiffnesses that degraded faster than those of a stress path that moved towards the compression side. The type of approach stress path they used, though, had also a lower angle of rotation for the stress path that moved towards the failure line and the two effects might therefore have been superimposed. The results discussed in Chapter 8 demonstrated that the effects of the angle of rotation and the effects induced by the presence of the failure line, can cancel each other out when they have opposite effects.

9.4 *Effects of angle of rotation on the kinematic surfaces*

The results of the probes described above were also used to investigate the effects that creep and angles of rotation produced on the yield surfaces. The results of the analyses conducted in Chapter 8 will be used here for comparison. Samples 17SH and 17.3SH belong to the lithological Sub-Unit $B_{2(b)}$, for which no other samples were tested at small strains, but the results of the analyses discussed in Chapters 7 and 8 suggest that similarities could be found between this sub-unit and the others, particularly in a normalised plane.

9.4.1 Shear modulus

Bender element tests were carried out before each shear probe and the results are summarised in Table 9.4. The shear moduli for Samples 17SH and 17.3SH are slightly different, probably due to inhomogeneities between the two samples, but, after the different consolidation stress paths, the shear moduli G_{hh} and G_{hv} did not change greatly in either of the samples. The measurements of the moduli are qualitatively similar to those described in Chapter 8 for samples from other units and the two interpretation methods used showed perfect agreement in the results. The values measured are consistent with those found for other lithological units and with the values expected for samples from this depth.

9.4.2 Elastic surface

In Figures 9.13-9.14, the stress-strain curves used to identify the elastic yield surface Y_1 are shown. The identification of the yield stresses was not easy, particularly for probes 17.3-105°$_c$ and 17.3-75°$_c$, and separate analyses of the radial strains and the Young's moduli supported the suggested values, which are tentatively indicated by arrows in the figures. In Figure 9.15 those values are plotted in a plane of stresses $\Delta p'$-Δq and the Y_1 surface for samples from Sub-Unit $B_{2(a)}$, identified in Chapter 8, is also added to the graph for comparison. As discussed in Chapter 8, the Y_1 surface of the Sub-Unit $B_{2(a)}$ was found from probes on samples that had been subjected to an approach stress path that, while re-tracing the geological history of the clay, created a minimum disturbance to its structure. These samples were also allowed to creep until the creep rates had

reduced to negligible values before probing. In the investigation on the recent stress history, those probes that had a short approach stress path and creep rates reduced before shearing, 17-23°$_e$ and 17-157°$_e$, are most similar to the probes performed on the samples from the Sub-Unit $B_{2(a)}$, and they seem to yield at the same values at which the samples from the Sub-Unit $B_{2(a)}$ yielded. The angles of rotation from the approach stress path have no effects on the yielding of these samples.

The probes that had been subjected to larger strains before shearing with creep rate reduction, 17.3-L30°$_e$ and 17.3-L150°$_e$, yielded at slightly larger stresses than those measured for Sub-Unit $B_{2(a)}$, particularly Probe 17.3-L150°$_e$, with the larger angle of rotation. The difference, though does not seem to be large and might be due to the strain rate effects, as these probes were performed at strain rates around ten times faster than those used for the probes in Sub-Unit $B_{2(a)}$.

The probes that had no creep rates reduction, Probes 17.3-75°$_c$ and 17.3-105°$_c$, yielded at larger stresses than those found for the Sub-Unit $B_{2(a)}$ and at different values for the two angles of rotations. The identification of the yield stresses on these probes was not easy and the suggested values might not be the true yield stresses because they are affected by creep strain effects.

In Figure 9.16, the yield points are plotted in a plane of stresses normalized by the initial effective stress p'$_o$. In this plane, a unique Y_1 contour was found for all the lithological units (Section 8.5.2). Only the yield stresses of the probes 17-23°$_e$ and 17-157°$_e$, though, plot on this contour, whereas the yield stresses of the other probes plot further out.

The axial strains at which the yields occurred are similar to the yield strains found for all the other units, with the exception of the cases in which the creep rates were not allowed to reduce. As mentioned before, this is due to the interaction of creep strains on the strains developed by the loading.

The undrained Young's moduli found from the probes are included in Table 9.4. Consistently with the discussion for the Y_1 yield stresses, the probes with the

short approach stress path and the creep reduced (17-23°$_e$ and 17-157°$_e$) show virtually no difference in the E^u_v values for the two angles of rotation. The other probes, performed on a different sample, show similar values of E^u_v except for the probe at 75° rotation with no creep allowed, which shows a lower E^u_v. The value identified for this probe, though, as mentioned above, is not the true undrained Young's modulus because of the influence of creep strain effects. This is confirmed by the fact that the shear moduli, which were calculated with the bender elements and were not affected by strain rates, are similar. The elastic parameters derived from the probes are not sufficient to calculate the equivalent shear moduli to be compared with the measured values.

9.4.3 Y_2 surface

The yield stresses for the Y_2 surface were identified as described in Chapter 8 from the change in deviatoric stress with pore pressure. The graphs are shown in Figures 9.17-9.19 and the stresses identified are plotted in the stress plane $\Delta p'$-Δq in Figure 7.20. The Y_2 surfaces of the Sub-Units$B_{2(c)}$ and $B_{2(a)}$ are also included in the graph. The Y_2 yield points for the Samples 17SH and 17.3SH seem to plot between the surfaces of the other two sub-units, which was expected considering the depth of these samples. However, in the probes where the sample had been taken to relatively large strains during the approach stress path, the Y_2 yields, for both angle of rotation 30° and 150°, plot together at slightly lower stresses, suggesting a reduction of the Y_2 region caused by the approach path strains. In Figure 9.21 the normalized Y_2 contour is shown, which was found to be unique for all the lithological units. The probes that had been subjected to short approach stress paths plot on this contour, while the probe that was subjected to a long approach stress path plots at lower stresses. As for Y_1, the axial strains associated to the Y_2 yields are similar to those found for other lithological units.

9.4.4 Effect of creep

The comparison between the results from probes that differed only in the creep rates before shearing suggests interesting features for the sample behaviour with regard to bubble type models. In Probes 17-23°$_e$ and 17-157°$_e$, the creep rates were completely reduced before shearing and no differences could be

noticed between the location of the Y_1 and Y_2 yield stresses and the elastic parameters for both angles of rotation. In Probes 17.3-75°$_c$ and 17.3-105°$_e$, instead, the reduction of the creep rates had not been allowed before shearing and the yielding for both the Y_1 and the Y_2 regions occurred at larger stresses for the probe at 105° rotation than for the probe at 75° rotation. These features are consistent with the behaviour hypothesized in the bubble model, where the elastic bubble is dragged with the stress point. It is thought that the elastic bubble re-centres around the current point when the stresses are held constant to allow creep. In probes where creep had been allowed before shearing, the Y_1 surface is expected to be centred and symmetric around the stress state, and in each direction the yield should therefore be at the same distance from the initial stress state. In the probes where the creep had not been allowed, instead, the Y_1 surface is expected to be asymmetric around the initial stress point and orientated towards the direction of the approach stress path. In this case, for 150° rotation, the stress state moves inside the Y_1 bubble towards the direction of the approach stress path and therefore towards the larger side of the Y_1 bubble. This probably caused the increased dimension of the Y_1 for the 150° rotation. The Y_2 surface, instead, seems only to be affected by the destructuration strain applied to the samples that result in a reduced dimension of the surface.

Test 17SH				
Approach stress path	ε_v [%]	ε_a [%]	ε_r [%]	ε_s [%]
C-O	0.006	0.004	0.001	0.002
B-O	-0.004	-0.005	0.0006	-0.004

Table 9.1: Strains developed during the approach stress paths for Probes 17-23°$_e$ and 17-157°$_e$ (refer to Figure 9.1)

Test 17.3SH, approach stress path below Y_2				
Approach stress path	ε_v [%]	ε_a [%]	ε_r [%]	ε_s [%]
A-O'	0.021	0.019	0.001	0.012
B'-O'	-0.005	0.0042	0.0001	0.0001

Table 9.2: Strains developed during the approach stress paths for Probes 17.3-75°$_c$ and 17.3-105°$_c$ (refer to Figure 9.5)

Test 17.3SH approach stress path outside Y_2				
Approach stress path	ε_v [%]	ε_a [%]	ε_r [%]	ε_s [%]
C"-O"	-0.17	-0.08	-0.04	-0.02
B"-O"	0.2	0.14	0.03	0.07

Table 9.3: Strains developed during the approach stress paths for Probes 17.3-L30°$_e$ and 17.3-L150°$_e$ (refer to Figure 9.9)

Approach stress path	Creep	Probe	G_{hh} [MPa]	G_{hv} [MPa]	E^u_v [MPa]
Short	*	17-23°$_e$	146	72	174
	*	17-157°$_e$	148	71	189
		17.3-75°$_c$	130	64	134
		17.3-105°$_c$	129	64	217
Long	*	17.3-L30°$_e$	128	66	195
	*	17.3-L150°$_e$	126	65	215

Table 9.4: Elastic parameters for probes on Samples 17SH and 17.3SH

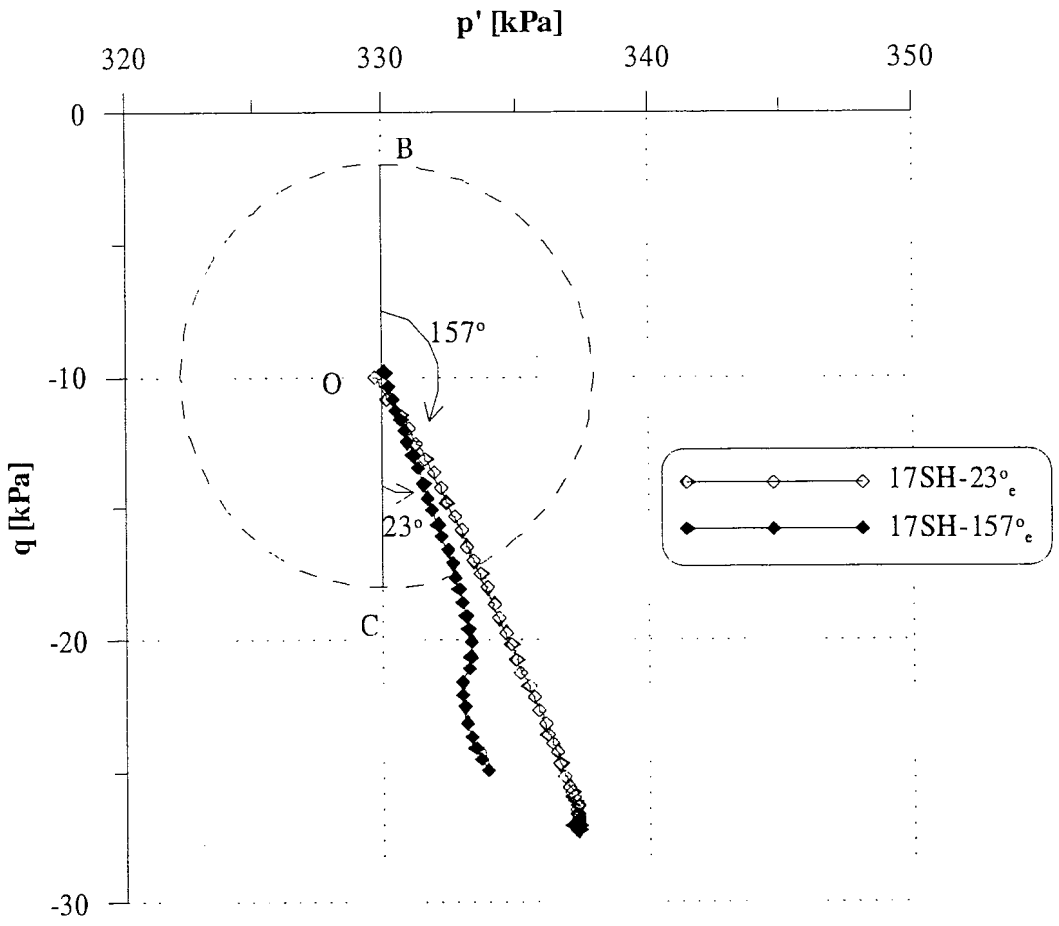

Figure 9.1: Approach stress paths and shear probes for Sample 17SH

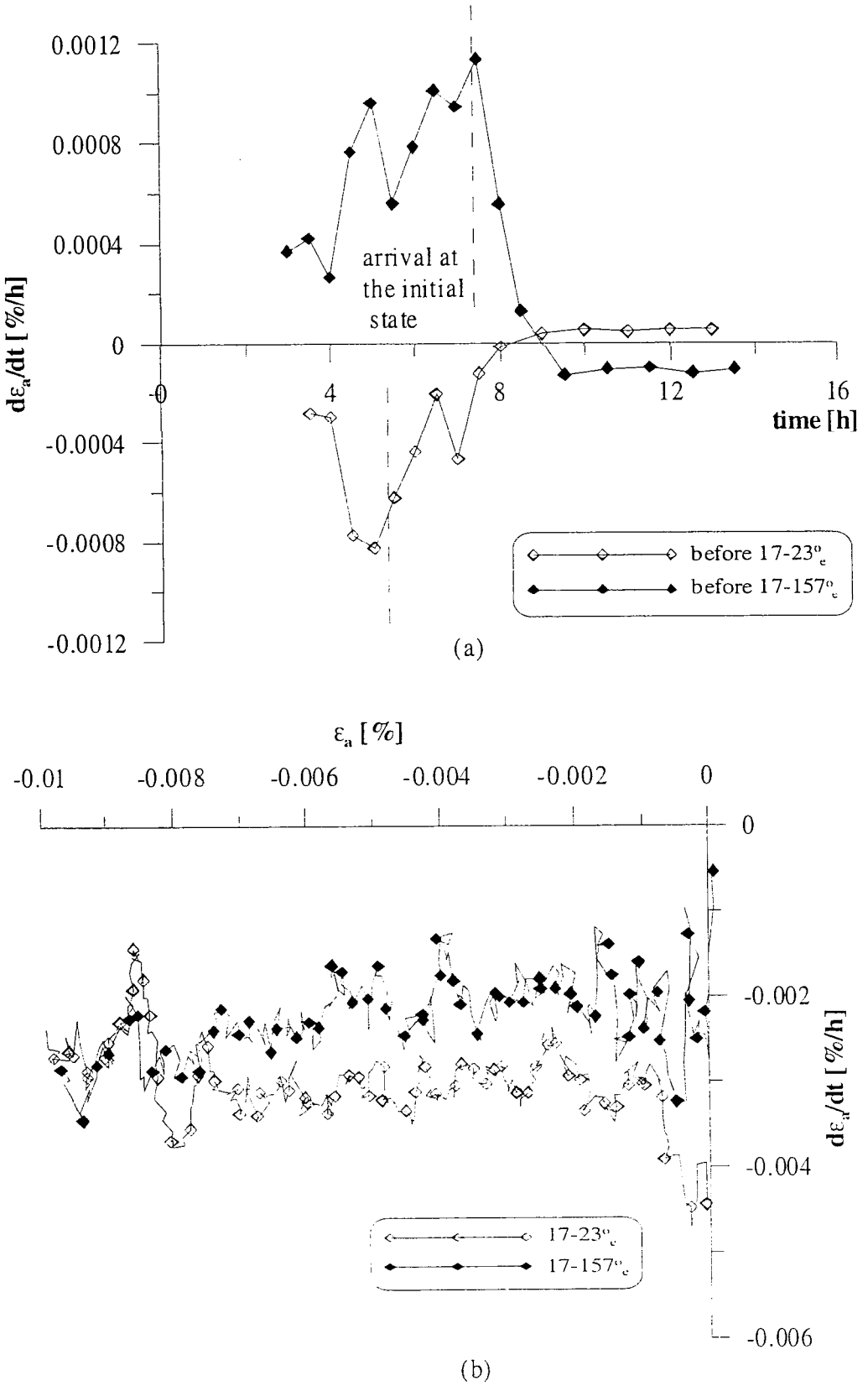

Figure 9.2: Strain rates for Sample 17SH (a) creep strains before the shear probes (b) strain rates during the probes

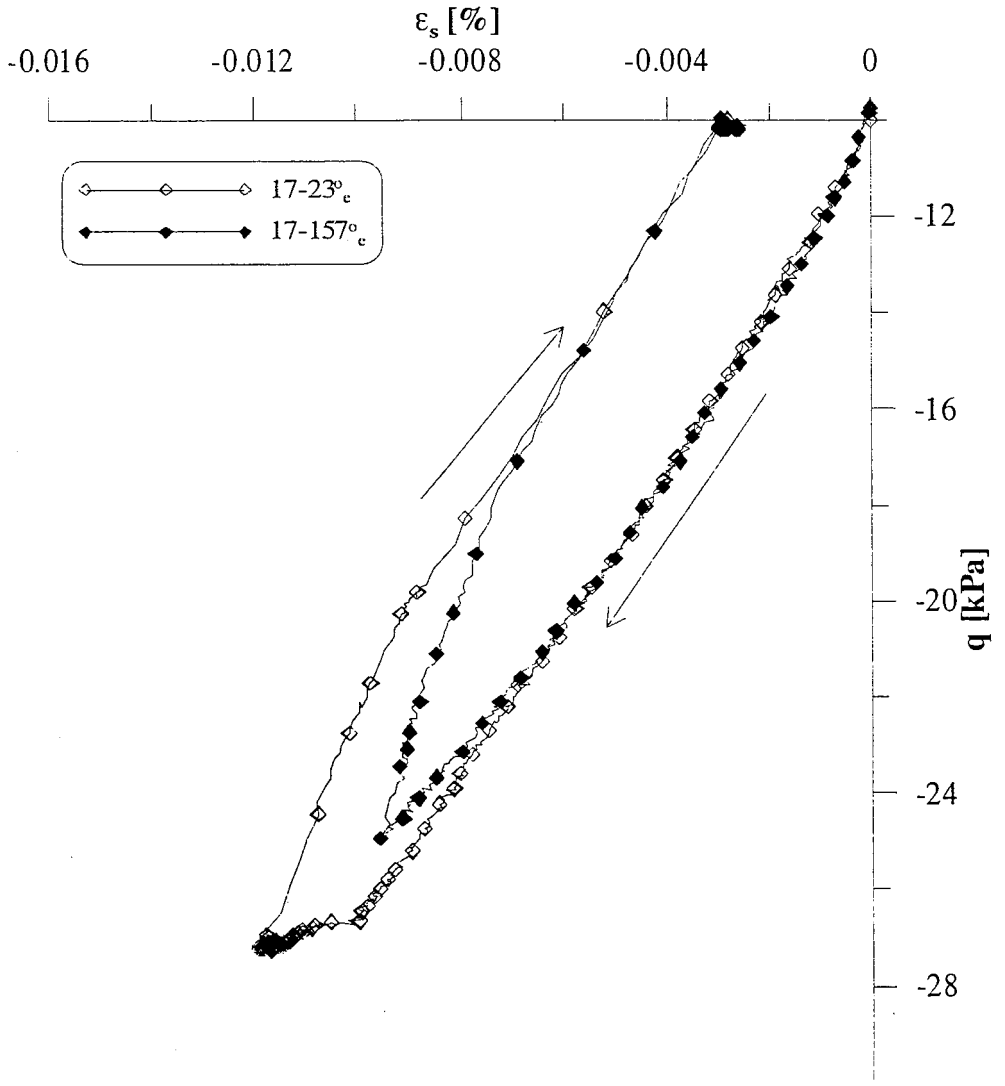

Figure 9.3: Stress-strain curves for the probes on Sample 17SH after a short approach path

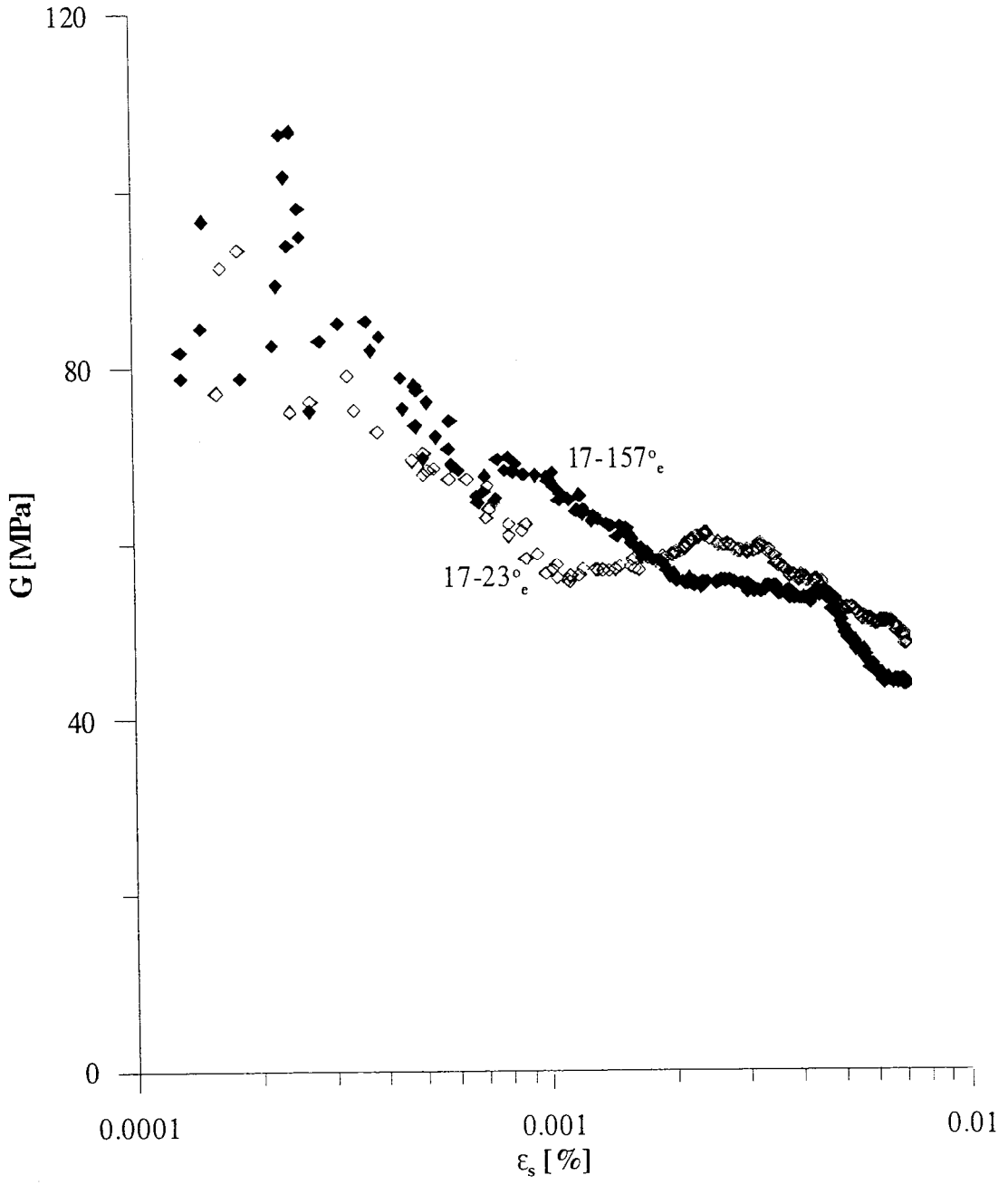

Figure 9.4: Shear stiffness for the probes on Sample 17SH

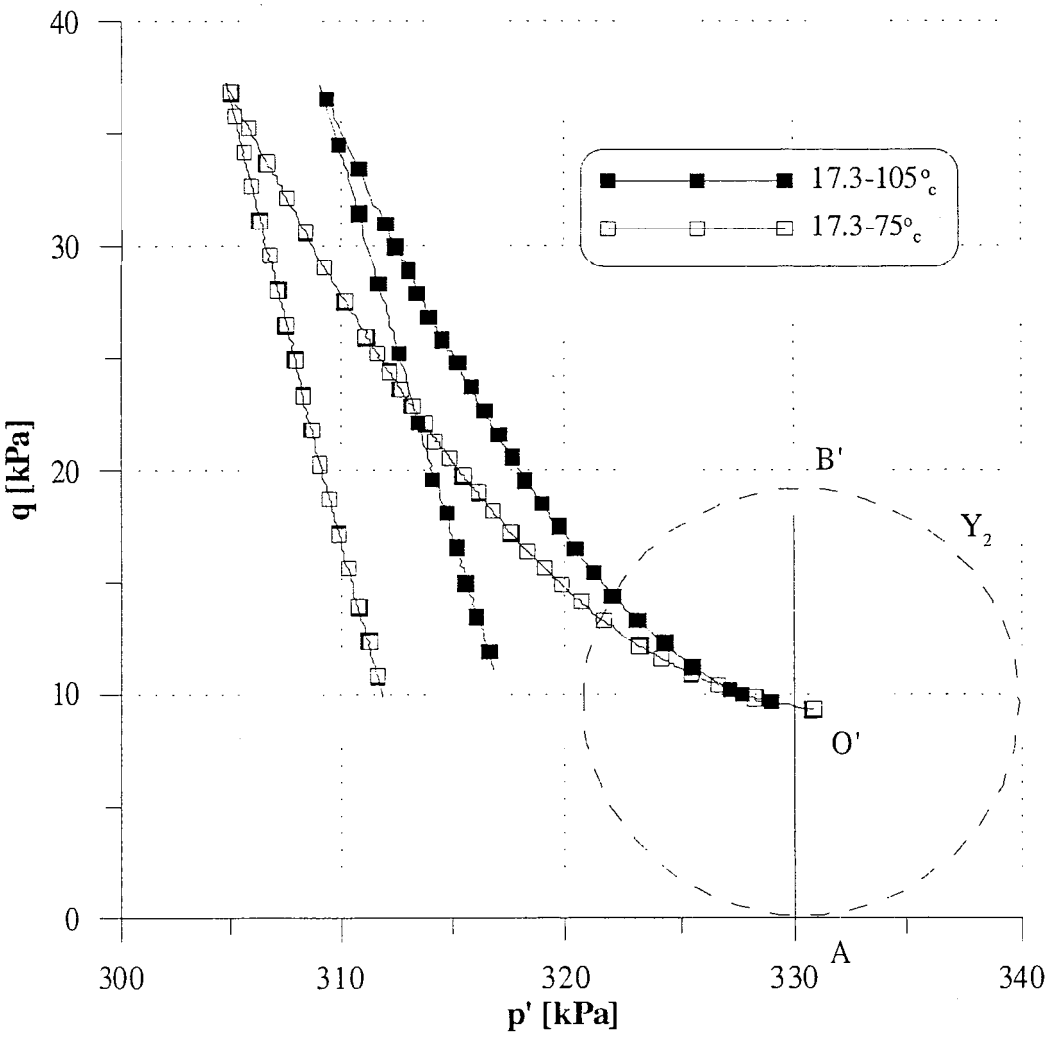

Figure 9.5: Short approach stress paths and shear probes for Sample 17.3SH

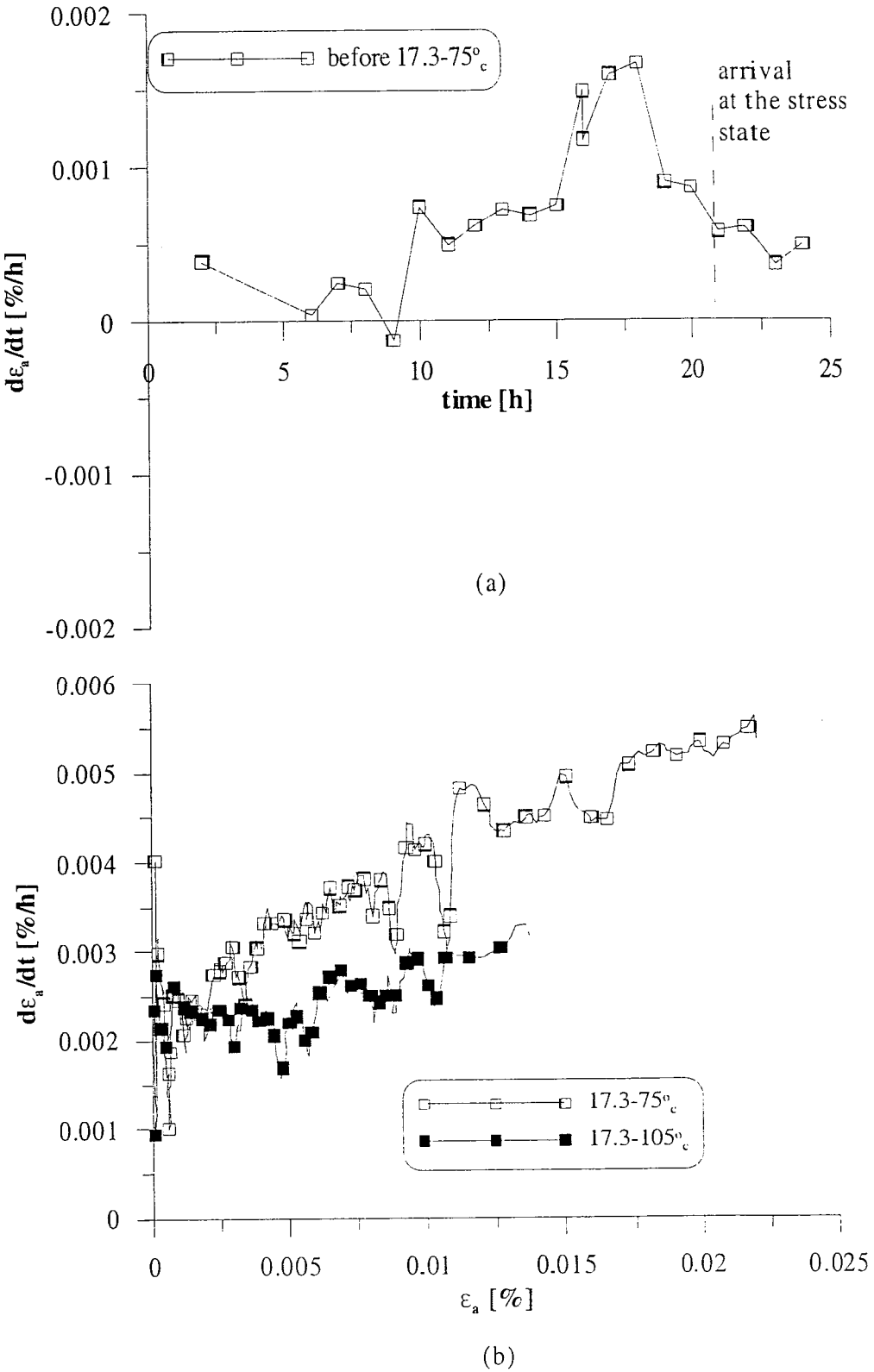

Figure 9.6: Strain rates for the short approach stress paths of Sample 17.3SH (a) creep rates before the shear probes (b) strain rates during the probes

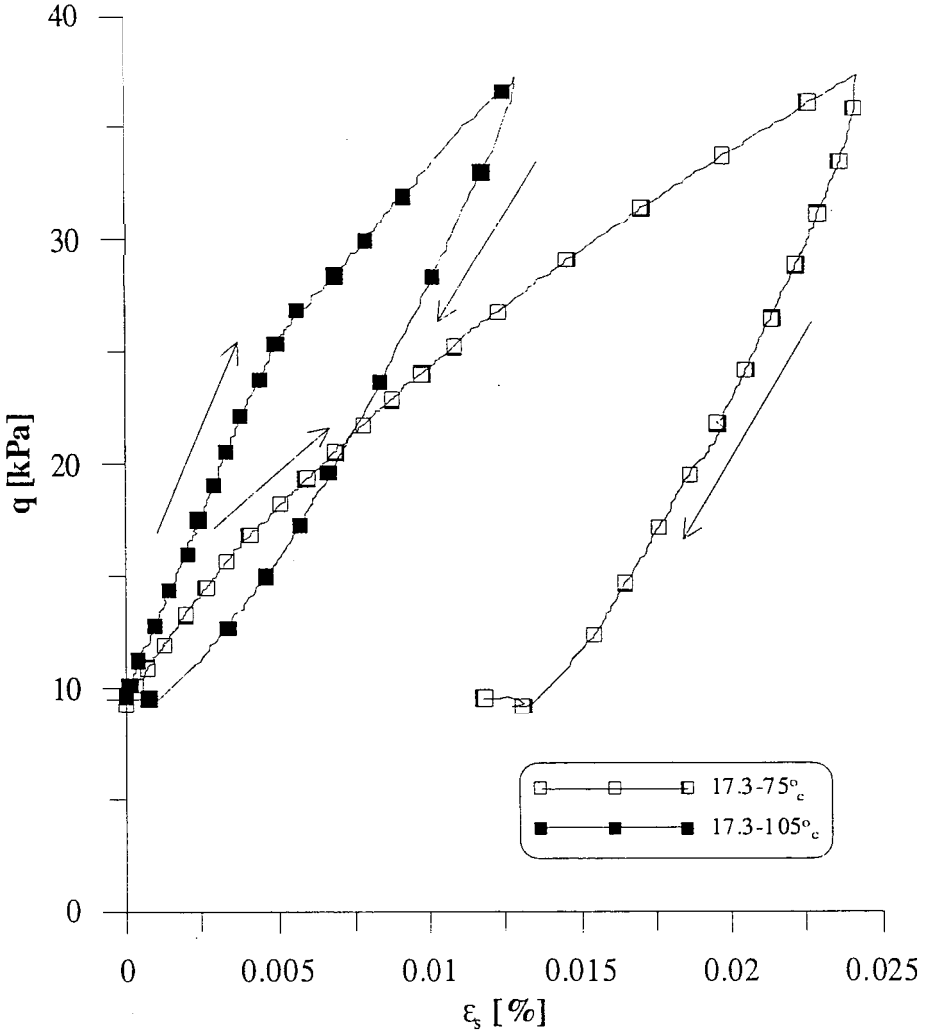

Figure 9.7: Stress-strain curves for the probes within the Y_2 region of Sample 17.2SH

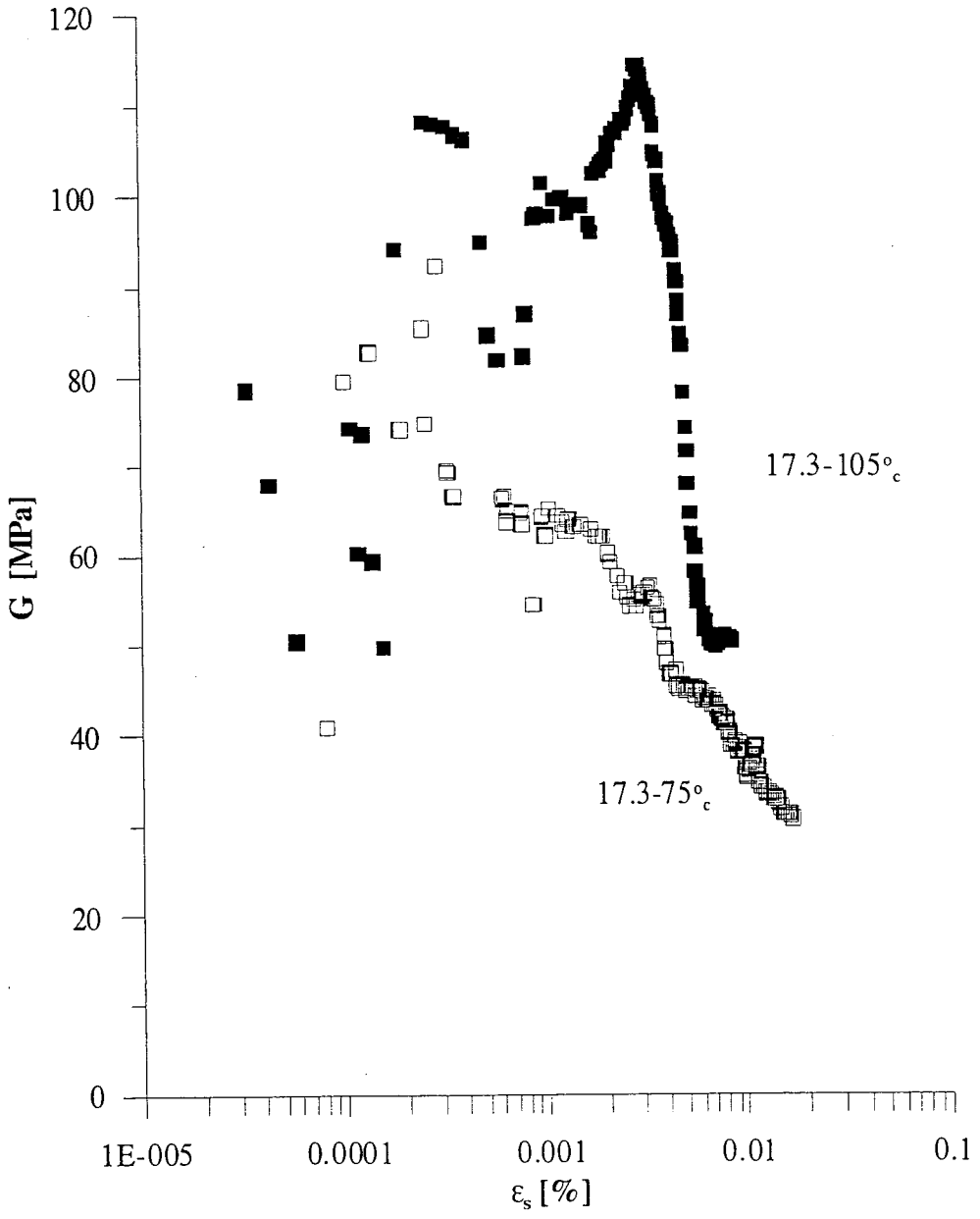

Figure 9.8: Stiffness degradation curves for the probes within the Y_2 region of Sample 17.3SH

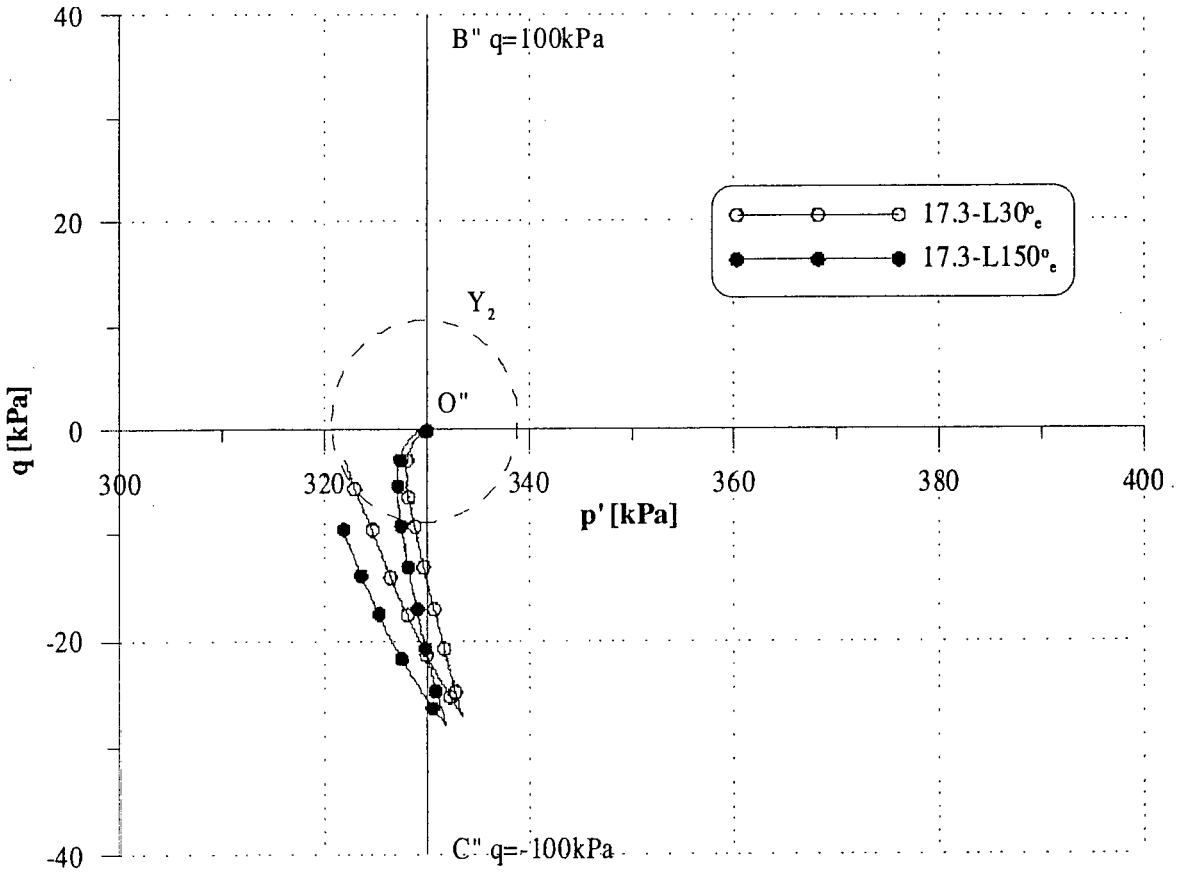

Figure 9.9: Approach stress paths above Y_2 and shear probes for Sample 17.3SH

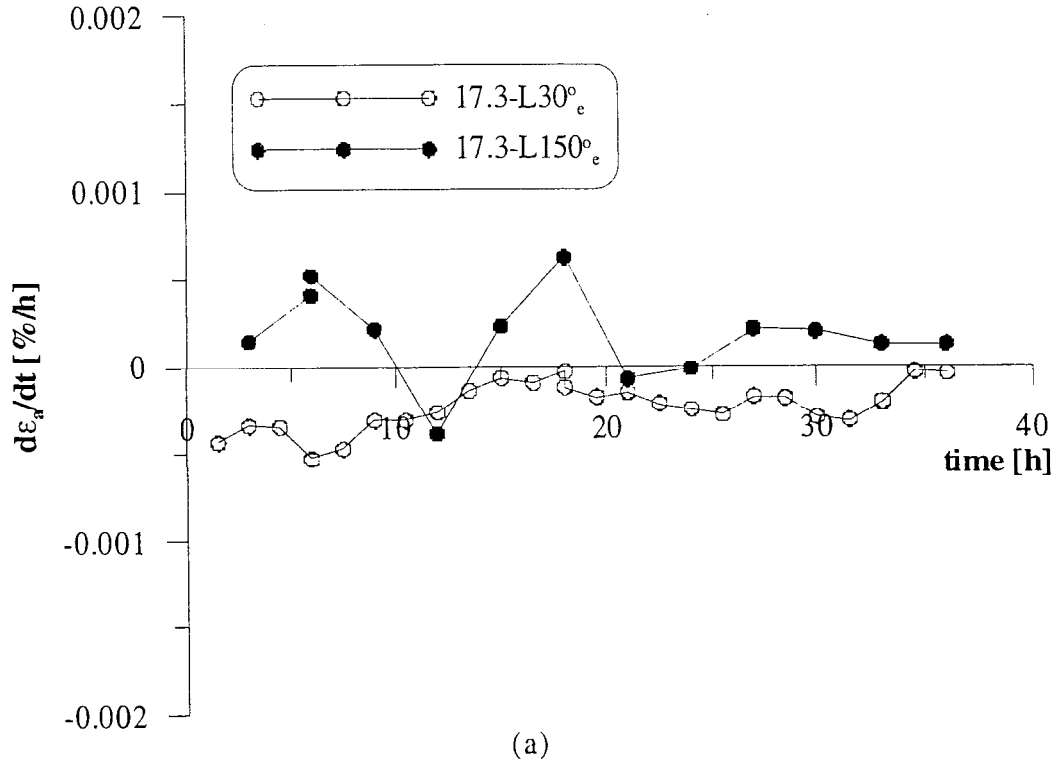

(a)

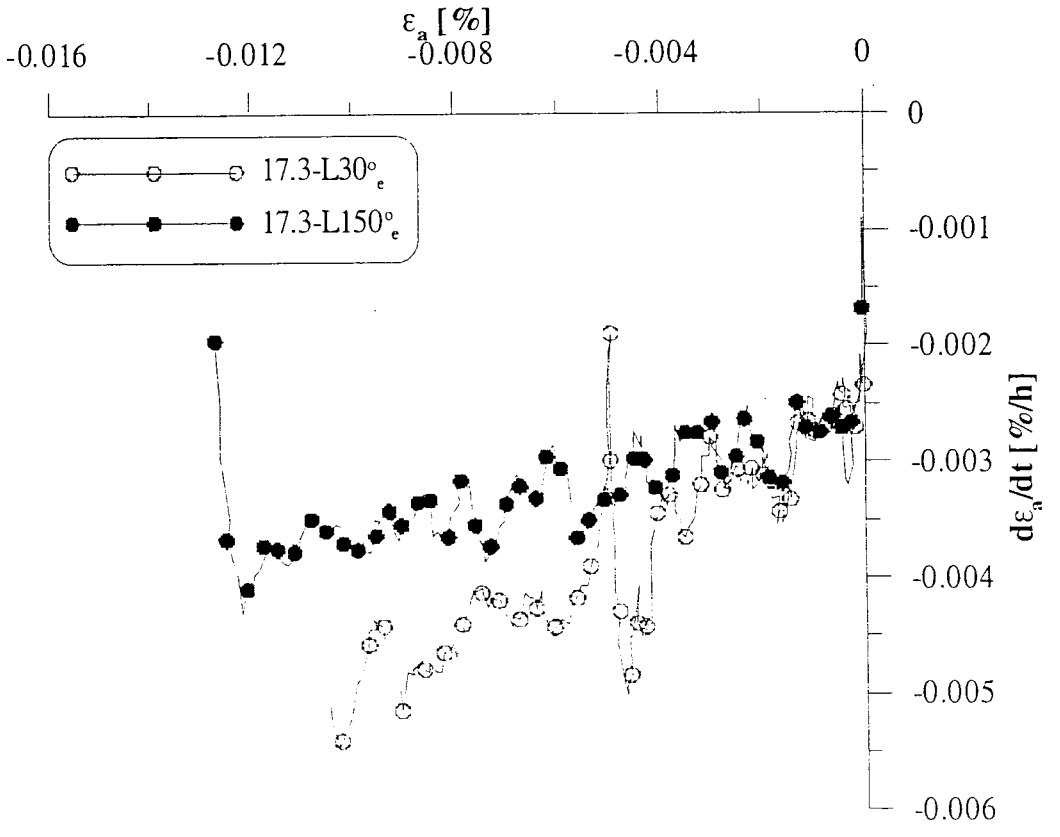

(b)

Figure 9.10: Strain rates for Sample 17.3SH subjected to a long stress path (a) creep strain rates before probes (b) strain rates during the probes

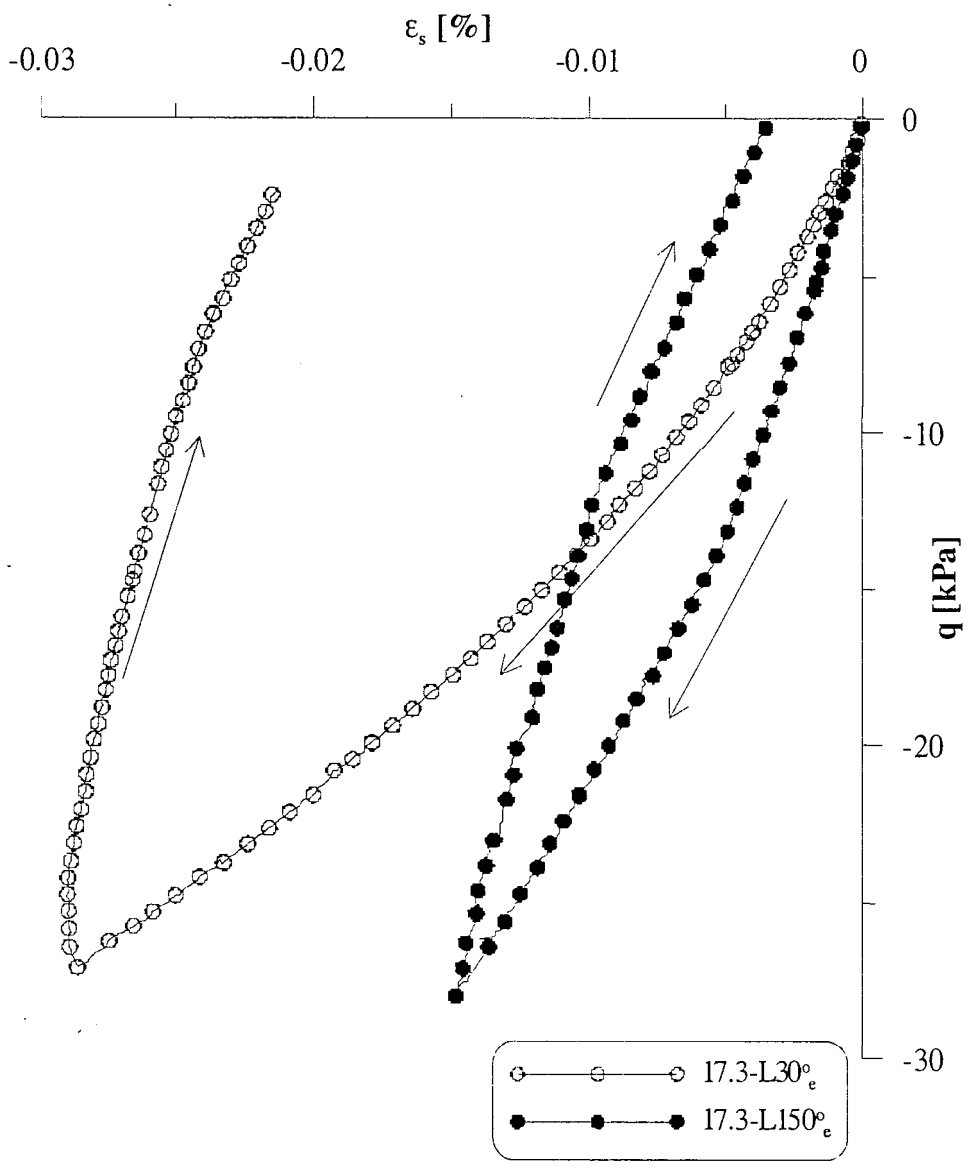

Figure 9.11: Stress-strain curves for the shear probes on Sample 17.3SH after long approach stress path

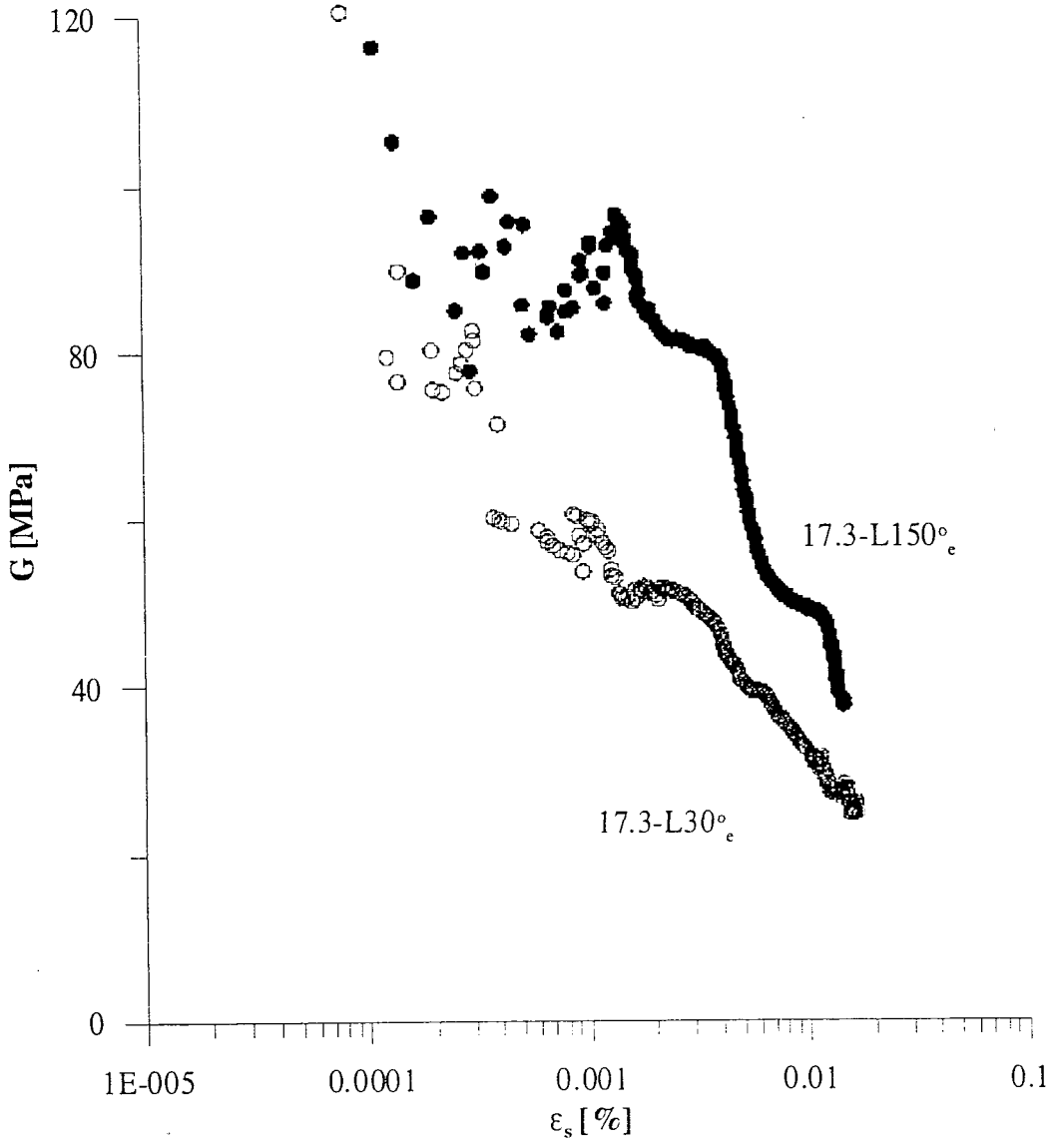

Figure 9.12: Stiffness degradation curves for the probes on Sample 17.3SH after a long stress path

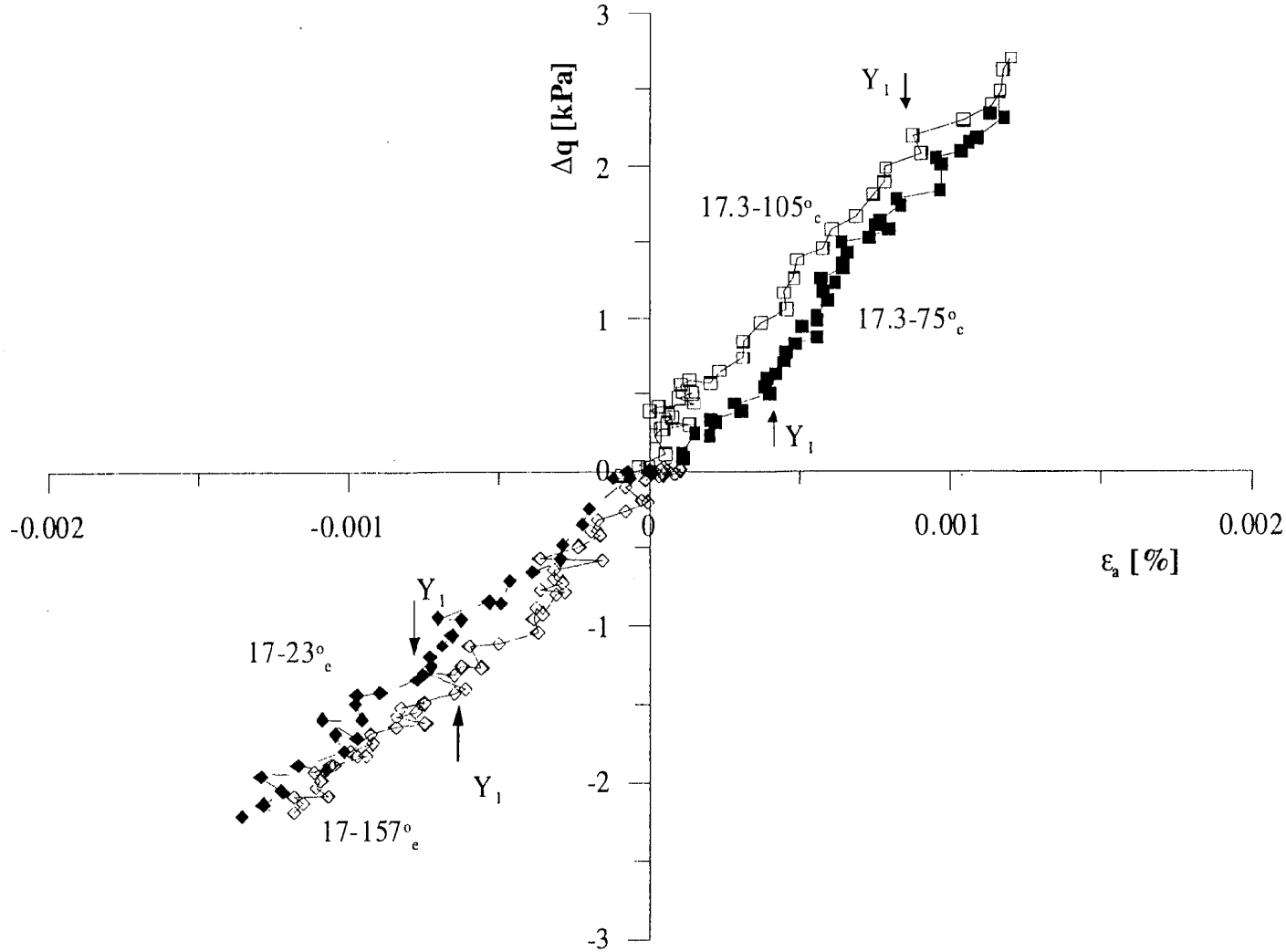

Figure 9.13: Yield points for the linear elastic region of samples subjected to short approach stress paths

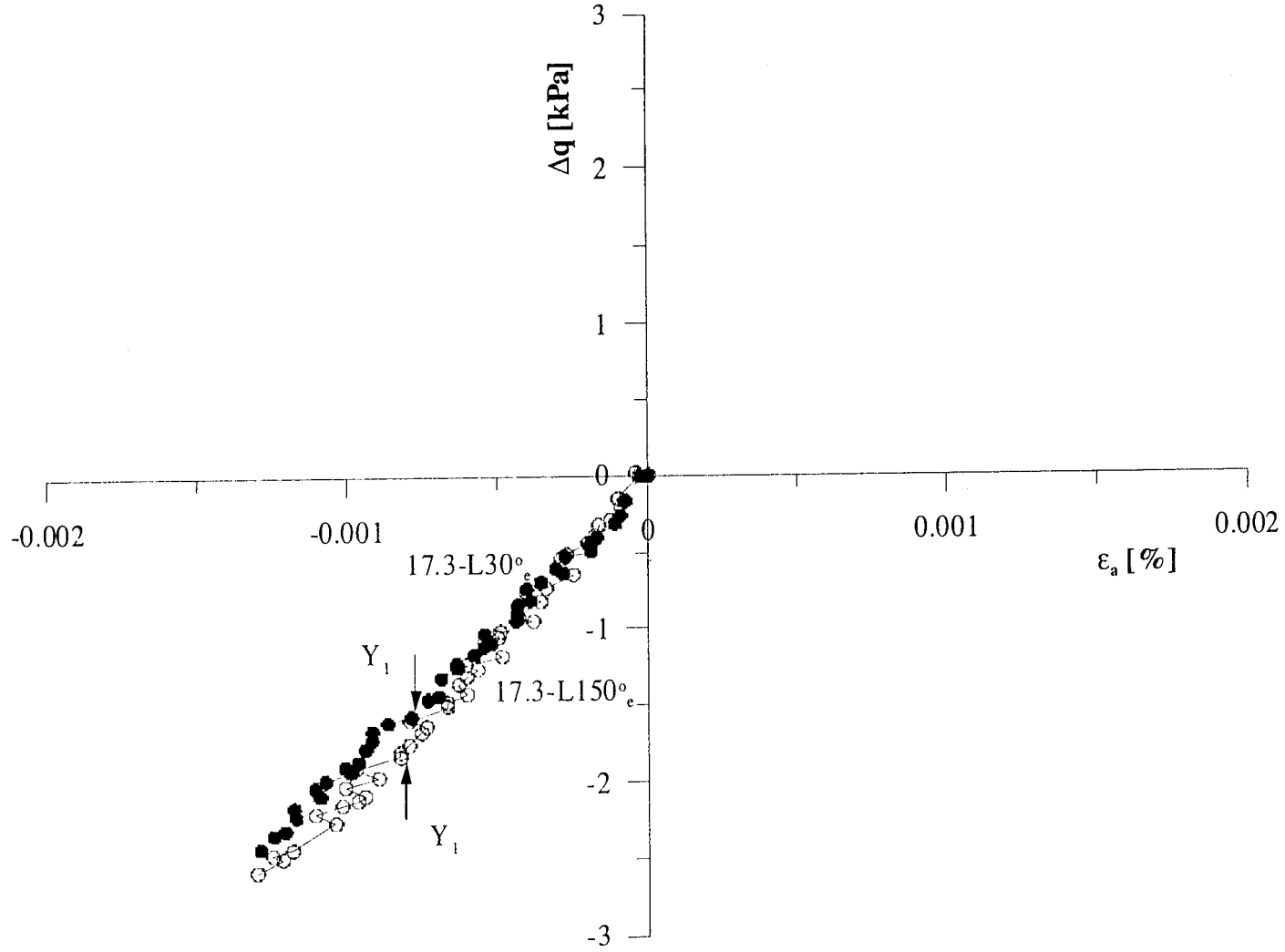

Figure 9.14: Yield points for the linear elastic region of Sample 17.3SH subjected to a long approach stress path

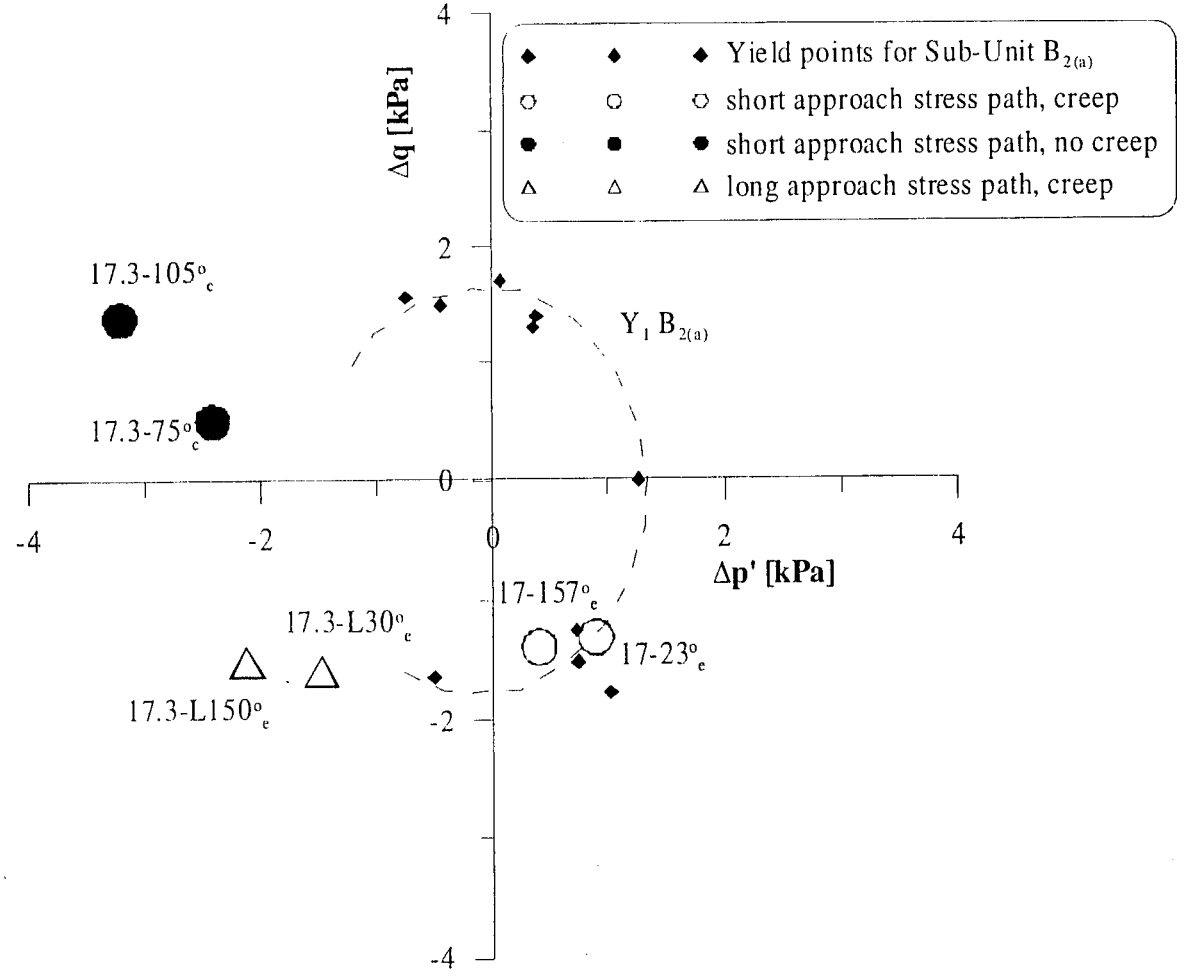

Figure 9.15: Yield stresses for the probes on Samples 17SH and 17.3SH and the contour of the elastic region for Sub-Unit $B_{2(a)}$

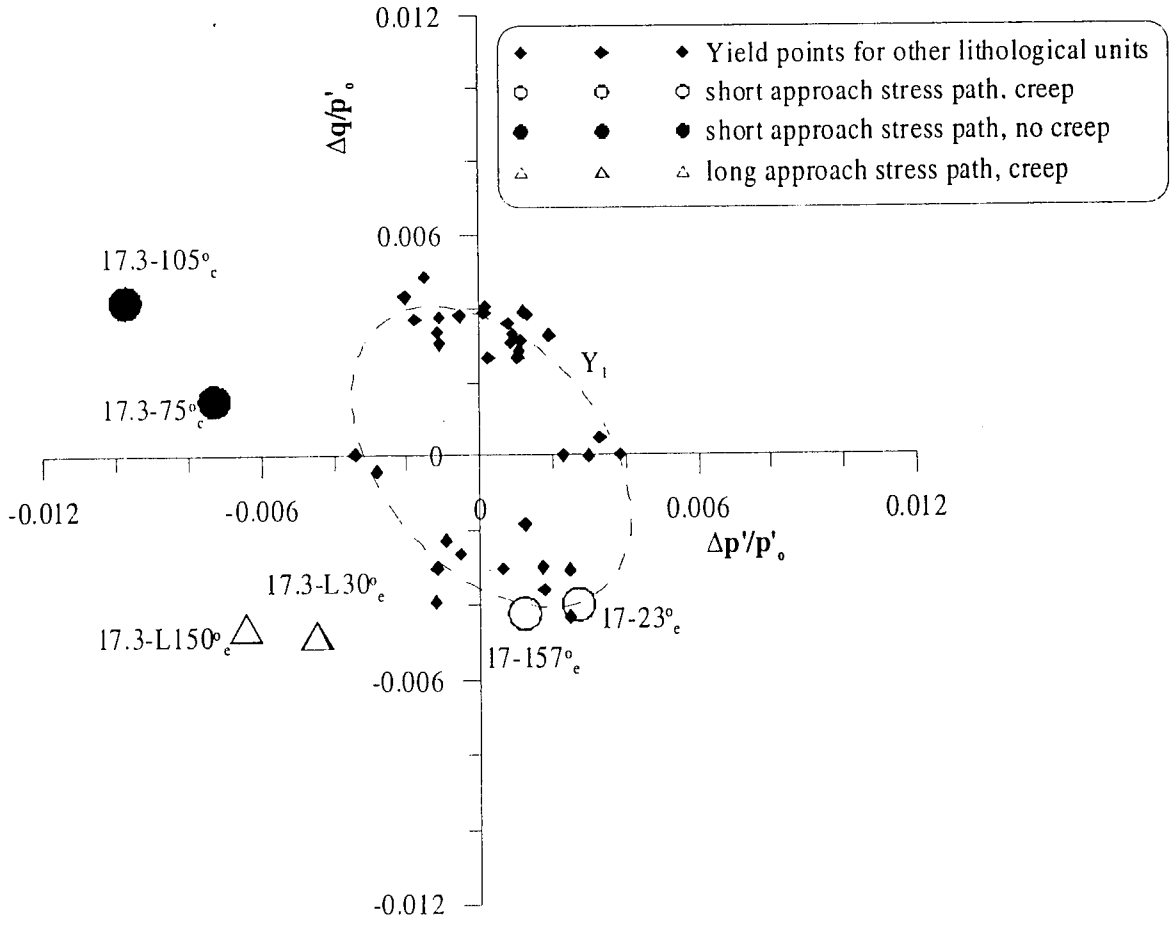

Figure 9.16: Normalized yield stresses for the probes on Samples 17SH and 17.3SH and normalized contour of the elastic region for Sub-Unit $B_{2(a)}$

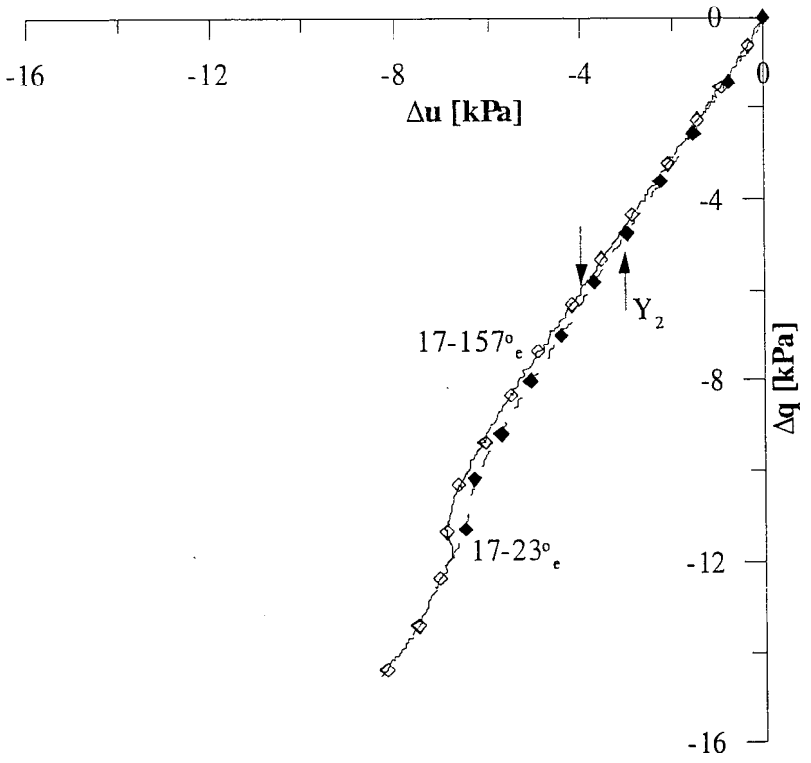

Figure 9.17: Y_2 Yield points for the probes on Sample 17SH

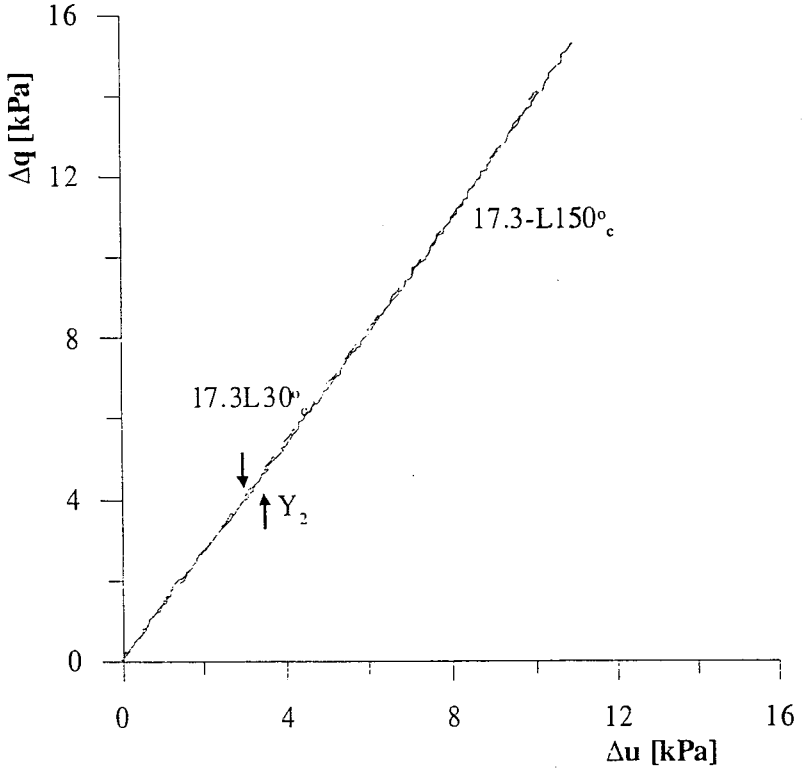

Figure 9.18: Y_2 Yield points for the probes on Sample 17.3SH where the creep was not allowed

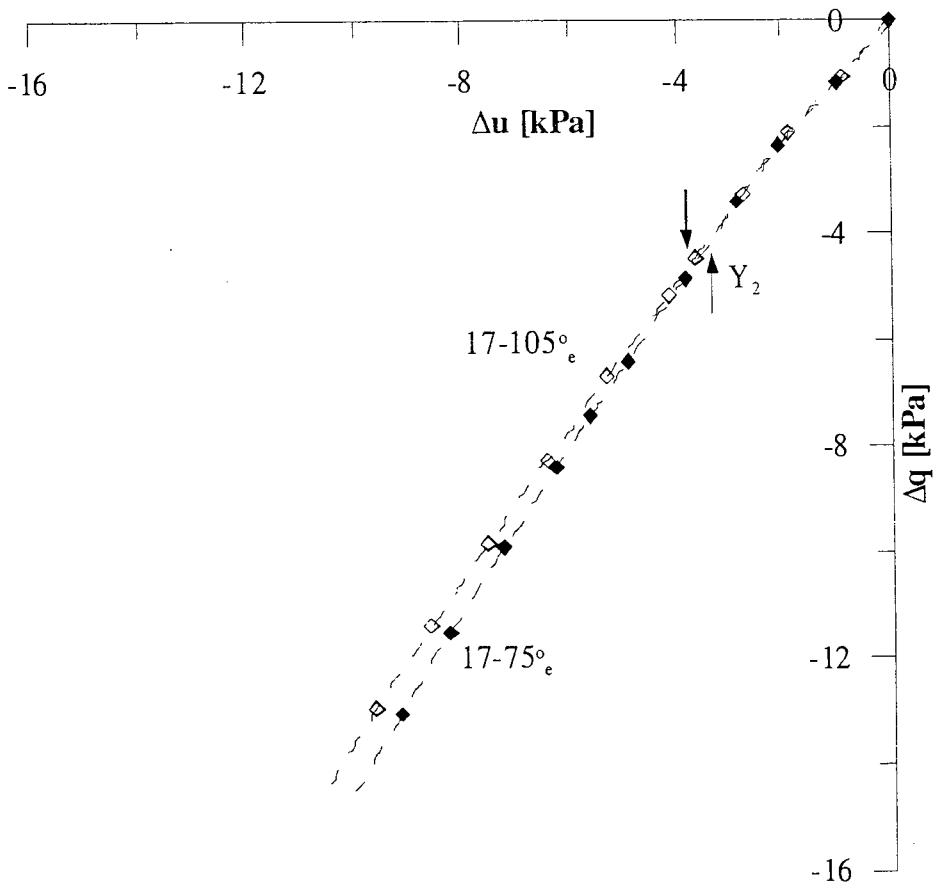

Figure 9.19: Y_2 Yield points for the probes on Sample 17.3SH subjected to long approach stress path

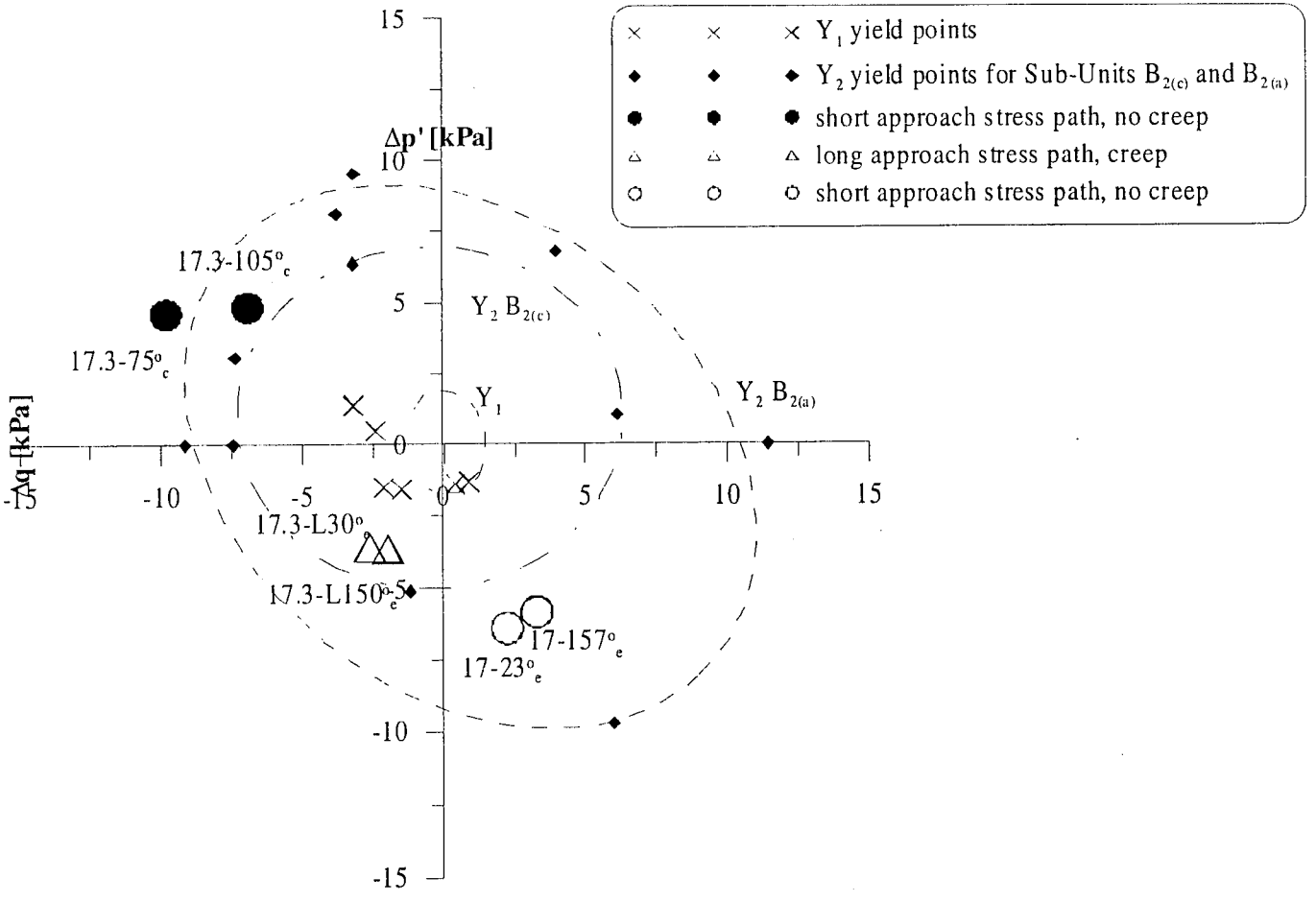

Figure 9.20: Y_2 yield points for the probes on Samples 17SH and 17.3SH and the contour of Y_2 for Sub-Unit $B_{2(a)}$

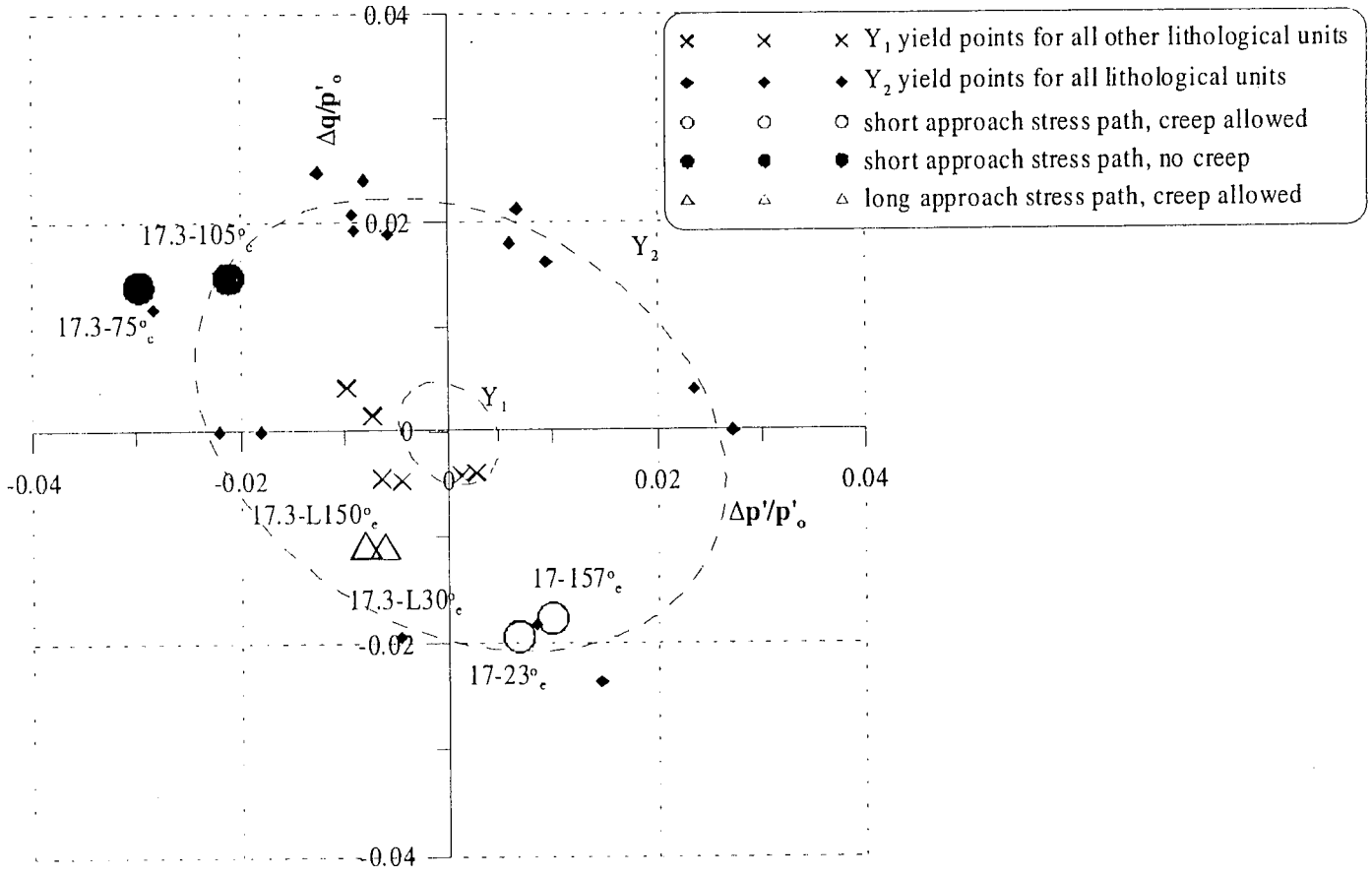

Figure 9.21: Normalized yield of the Y_2 region for the probes on samples 17SH and 17.3SH and normalized contour of the Y_2 region for the other lithological units

10 CONCLUSIONS

This research aimed at finding a framework for the London Clay relating the engineering proprieties of this material to its geological features. Samples from different depths were tested, belonging to different lithological strata of the London Clay. For each stratum, the large and small strain behaviour was investigated, which involved triaxial and oedometer tests on natural and reconstituted samples and the use of high accuracy instrumentation for the measurements of strains. A comparison between the mechanical responses of samples from different lithological units allowed the identification of a relationship between the engineering properties and the geology of London Clay.

Five main lithological units, C, B_2, B_1, A_3 and A_2 exist at Heathrow T5 (Hight et al., 2003; Mannion, 2005), but this research concentrated on Units C, B_2 and A_3. No samples from Unit B_1 were available for testing, as the nature of this layer usually does not allow the recovery of good quality samples. For Unit A_2, only oedometer tests were performed. Three main sub-units were also identified in Unit B_2, $B_{2(c)}$, $B_{2(b)}$ and $B_{2(a)}$. The differences in the lithology of the clay were revealed by both the nature and the structure of the clay in the different units. The nature of the clay influenced its intrinsic behaviour, but did not seem to affect its intact behaviour as much as the structure of the clay, which was dominant in determining the differences in the mechanical response of samples from different lithological units.

The differences in the nature of the clay from different lithological strata were revealed particularly by the grading curves and also by the Atterberg limits and water content distributions with depth, although slightly less clearly. Within each stratum, the characteristics of the clay seemed fairly uniform and showed similarity in mineralogy and grading, so that a unique NCL* and CSL* could be found for each unit. The location of the NCL*s and CSL*s depended on the stratum, although NCL* and CSL* had the same offset for all strata. The more plastic units had an NCL* and CSL* plotting above the others in the v-lnp'

plane, however, the parameters λ, κ and M and C^*_c and C^*_s were unique for the clay, regardless its lithology, so that the NCL* for all strata were parallel. In Unit B_2, the gradings, the index properties and microfossil analyses (Mannion, 2005) highlighted the presence of a stratum, $B_{2(c)}$, with different characteristics from the lower strata, probably as result of the vicinity of the lithological boundary. This was reflected in a different NCL* for this sub-unit.

The mechanical response of undisturbed samples did not seem greatly influenced by its nature, but was dominated by the structure of the clay from the different strata. The microstructure of samples from Unit C, Sub-Unit $B_{2(a)}$ and Unit A_3 was investigated with SEM and showed that a probable originally flocculated fabric for this clay developed into a cardhouse fabric at shallower depths and into a bookhouse fabric at greater depths, perhaps as result of compression. Domains with sub-horizontal orientations were typical of the deepest Unit A_3 and probably were responsible for an increase in the horizontal stiffness of the clay from deeper strata. A compact, but not orientated structure characterised Unit B_2, and an open structure emerged for the shallowest Unit C, for which SEM, X-ray, and microfossil analyses also confirmed that the clay had experienced no weathering processes. The microstructure of the clay explained its small strain behaviour being stiffer horizontally than vertically. The ratio between the horizontal and vertical moduli increased with depth, though, consistently with the sub-horizontal orientation of the particle domains in deeper units.

The presence of coarser grains seemed to characterise Units C and A_3, for which the index properties showed a similarity in nature, although X-ray diffraction analysis revealed similarities in the composition of Units C and B_2, which also showed similarities in their mechanical behaviour. In no unit could a general calcite coating be seen that would create a strong bonding between the particles and only localised calcite crystals could be identified in some strata, which could only provide a minor localised bonding for the clay. The compression behaviour of the intact samples in fact showed that the compression

curves did not converge towards the intrinsic compression lines but retaining stable elements of structure even at higher stresses and large strains.

Both the shearing and compression behaviour of the clay was affected by the structural differences between the units, although these differences were more evident in compression and in the strength envelopes at higer pressures. Samples from units having an open structure, such as Units C and B_2, were more compressible and had lower strengths than samples from units with a more packed and orientated structures, such as Unit A_3, despite the similarity in nature between Units A_3 and C. Likewise, in Unit B_2, a fairly uniform behaviour could be found, with a unique compression curve and strength envelope, despite the presence of lithological sub-units having different index and intrinsic properties. The differences between the strength envelopes of the clay from different units at low pressures were not large and the intact SBSs plotted fairly close to the SBS*s. At higher pressures, though, the strength envelopes of clays with more orientated structure plotted above the envelopes of clay with the more open structure and the intact SBSs also extended well above the intrinsic SBS*.

These differences in the clay structure for the different units, however, were found to be not consistently represented by the Stress Sensitivity and the Void Index, which only seemed to reflect in the depth of the samples. A normalisation that accounts for the initial void ratio relative to the ICL shows that shallower samples have more structure than deeper samples, contradicting the stiffness and the strength behaviour of the clay. The structural features of such a clay, having a fabric dominated structure, seem more effectively represented by a new normalising parameter, e_n, that is calculated relative to the intrinsic swelling curves as well as the intrinsic compression line.

Structural changes to the intact clay were caused by swelling, but these only affected its compression behaviour inducing lower stress sensitivities and did not affect the strengths of the samples. Anisotropic stresses applied during compression to higher stresses did not seem to induce differences in the strength of the clay compared to isotropic compression.

At small strains, both the microstructure of the clay and the stresses applied influenced the clay behaviour, particularly its elastic parameters. The size of the kinematic surfaces, though, mainly depended on the consolidation pressures, so that, when the stresses were normalised by the initial state, unique kinematic surfaces Y_1 and Y_2 appeared for the clay for all strata. The region of purely elastic behaviour of London Clay did not exceed an overall radius of about 2kPa. Constant values of incremental strain energy were found to be associated with the yield surfaces.

Strain rate effects were found to influence slightly the behaviour at small strains, although undissipated pore water pressures had to be accounted for. In the study at small strains, creep rate effects were removed by allowing creep rates to reduce to negligible values before conducing any probes. The relationship between creep strains and strain developed during shearing was then analysed separately considering recent stress history effects. Stress history effects were found to be less important than strain history effects. A relationship could be found between the stress-strain behaviour of samples subjected to different stress path rotations, strains developed during the approach stress paths and creep strains. When the samples had not experienced large strains during the consolidation stress paths, then creep could erase the influence of the approach stress path on the outgoing stress path. However, when large strains developed during the approach stress path, stress history effects are evident and induce stiffer behaviour for the outgoing stress path having the larger angle of rotation from the approach stress path. In studying recent stress history effects the influence of other interacting parameters, such as the vicinity of the failure lines, had to be avoided.

The effect of fissures on the samples behaviour was analysed at both large and small strains,. The distribution of the fissures on site was not recorded in this study and only a post-test analysis of the fissures was conducted. From this analysis, there seemed to be a larger occurrence of samples that sheared along pre-existing fissures from Sub-Unit $B_{2(a)}$. Natural fissures were distinguished from fissures formed as consequence of drying during the sample preparation. Fissures due to drying did not affect the mechanical behaviour of the samples,

while natural fissures only affected the large strain behaviour if they were orientated in directions compatible with the shearing mode. The strength on fissures was lower than the intact strength, consistent with the literature, but these fissures did not seem to affect either the elastic parameters or the sizes of the kinematic surfaces.

High quality rotary core samples were used for most of the work and their behaviour was found to be similar to that of block samples. No sample size effects were also evident apart from the greater likelihood that larger samples would contain fissures.

10.1 Suggestions for future work

This research work has highlighted the importance of accounting for lithology when dealing with natural soils. An investigation of Unit A_2 at both large and small strain is currently being undertaken to complete the picture of the behaviour of the more common London Clay strata. The fissured nature of this material also suggested the need for an accurate investigation of the distribution of fissure in situ for a better understanding of the influence of fissures on the bulk behaviour of the clay. A new construction phase of Heathrow T5 will soon give the opportunity to complete this aspect of the work.

High pressure tests were attempted in this research, but the pressures used were not high enough to cause significant destructuration of this material, for which the use of even higher pressures is required.

Further research testing is required to provide more comprehensive data to examine soil behaviour on the wet-side (i.e. with normally consolidated samples).

An investigation on the stiffness of reconstituted samples with bender element tests is also currently being undertaken to enable normalisation of the results of natural samples.

REFERENCES

Abdulhadi N., Triaxial testing on reconstituted London Clay. . *MSc dissertation, Imperial College London, University of London.*

Al-Tabbaa A. (1987), *Permeability and stress-strain response of speswhite kaoline.* PhD Thesis, University of Cambridge.

Al-Tabbaa A. and Muir Wood D.M. (1989), An experimentally based bubble model for clay. *Numerical methods in Geomechanics NUMOG III, Elsevier Applied Science, pp.91-99.*

Amorosi, (2004), personal communication.

Amorosi A. and Rampello S. (1998), The influence of natural soil structure on the mechanical behaviour of a stiff clay. The geotechnics of Hard Soils-Soft Rocks, Evangelista & Picarelli eds Balkema Rotterdam, pp. 395-402.

Atkinson J.H., Richardson D. and Stallebrass S.E. (1990) Effect of stress history on the stiffness of overconsolidated soil, *Géotechnique, 40, No.4, pp.531-540.*

Atkinson J. H. (1973), *The deformation of undisturbed London Clay*, PhD. Thesis, Imperial College of Science, Technology and Medicine, University of London.

Baudet B. and Stallebrass S. (2004), A constitutive model for structured clays. *Géotechnique, 54, No.4, pp.269-278.*

Bjerrum L. (1967), Engineering geology of Norwegian normally-consolidated marine clays as related to settlements of buildings, *Géotechnique, 17, No.2, pp.81-118.*

Bishop, A.W. (1966), Soils and soft rocks as engineering materials. *Inaugural Lecture, Imperial College, University of London.*

Bishop A.W. and Henkel D.J. (1957), The measurement of soil properties in the triaxial tests, *Edward Arnold LTD, London.*

Bishop A.W., Webb D.L. and Lewin P.I. (1965), Undisturbed samples of London Clay from the Ashford Common shaft: strength-effective stress relationships, *Géotechnique, 15, No.1, pp.1-31.*

Bishop A.W. and Little A.L (1967), The influence of the size and orientation of the sample on the apparent strength of the London Clay at Maldon, *Essex. Proc. Geotech. Conf., Oslo, 1, pp.89-96.*

Bishop A.W. and Wesley L.D. (1975), A hydraulic triaxial apparatus for controlled stress path testing, *Géotechnique, 25, No.4, pp.657-670.*

Blyth F.G.H. and De Freitas M.H. (1984), A geology for Engineers, *Edward Arnold, 7th Edition.*

British Geological Survey (2004), Geology of London, Special Memoir 256,257,270 and 271 (England and Wales). Keyworth, Nottingham.

British Standard Institution (1990). Methods of test for soils for civil engineering purposes. BS 1377, British Standard Institution, London.

Burland J. B. (1990), On the compressibility and shear strength of natural soils. *Géotechnique, 40, No. 3, pp.329-378.*

Burland J.B. and Georgiannou V.N. (1991), Small strain stiffness under generalised stress changes. *Proc. 10th ECSMFE, Florence, Vol.1, pp.41-44.*

Burland J. B., Rampello S., Georgiannou V.N. and Calabresi G. (1996), A laboratory study of the strength of four stiff clays. *Géotechnique, 46, No.3, pp.491-514.*

Cafaro F. and Cotecchia F. (2001), Structural degradation and changes in the mechanical behaviour of a stiff clay due to weathering. *Géotechnique, 51, No.5, pp.441-453*

Calabresi G. and Scarpelli G. (1985), Effect of swelling caused by unloading in overconsolidated clays, *Proc. 11th ICSMFE, San Francisco 1, pp.411-414.*

Callisto L. (1996), *Studio sperimentale su un'argilla naturale: il comportamento meccanico dell'argilla di Pisa.* PhD Thesis, Univerista' La Sapienza, Rome.

Callisto L. and Rampello S. (2004), An interpretation of structural degradation for three natural clays. *Can. Getech. J., Vol.41, pp.392-407*

Casagrande A. and Carrillo, (1944), Shear Failure on Anisotropic Materials. *Proc. Boston Soc. of Civil Eng. Vol. 31, pp.74-87.*

Chandler R.J. (1966), The measurement of residual strength in triaxial compression, *Géotechnique, 16, No.3, pp.181-186.*

Chandler R.J. (1968), A note on the measurement of strength in the triaxial compression tests, *Géotechnique, 18, No.2, pp.261-266.*

Chandler R.J. (1972), Lias clay: Weathering processes and their effect on shear strength, *Géotechnique, 22, No.4, pp.403-431.*

Chandler R.J. (2000) Clay sediments in Depositional Basin: the Geotechnical Cycle. *Quart. Journal of Engineering Geology and Hydrogeology*, Vol.33, pp.7-39.

Chandler R.J. (2002) personal communication

Chandler R.J. and Apted J.P. (1988), The effects of weathering on the strength of London Clay, *Quart. Journal of Engineering Geology, London, Vol.21, pp.59-68*

Clayton C.R.I. and Heymann, G. (2001), Stiffness of geometerials at very small strains. *Géotechnique, 51, No. 3, pp.245-255*

Coop M.R. (2005), personal communication

Coop M.R. and Cotecchia F. (1995), The compression of sediments at the archeological site of Sibari. *Proc. 11th ECSMFE, Copenhagen 1, pp.19-26.*

Coop M.R., Atkinson J.H. and Taylor R.N. (1995), Strength, yielding and stiffness of structured and unstructured soils, *Proc. 11th ECSMFE, Copenhagen 1, pp.55-62.*

Costa Filho L.M. (1984) Technical note: A note on the influence of fissures on the deformation characteristics of London Clay. *Géotechnique, 34, No.2, pp.268-2672*

Cotecchia F. (1996), *The effects of structure on the properties of an Italian Pleistogene clay.* PhD Thesis, University of London.

Cotecchia F. (2003), Mechanical behaviour of the stiff clays from Montemesola Basin in relation to their geological history and structure *Characterization and Engineering Proprieties of Natural Soils, Tan et al. eds.*

Cotecchia F and Chandler R.J. (1997) The influence of structure on the pre-failure behaviour of a natural clay *Géotechnique, 47, No.3, pp.523-544.*

Cotecchia F and Chandler R.J. (2000), A general framework for the mechanical behaviour of clay *Géotechnique, 50, No.4, pp.431-447.*

Cuccovillo T. and Coop M.R. (1997), The measurements of local axial strains in triaxial tests using LVDTs. *Géotechnique, 47, No. 1, pp.167-171.*

Fearon R.E. and Coop M.R. (2000) Reconstitution-what makes an appropriate reference material? *Géotechnique, 50, No.4, pp.471-477.*

Fookes P.G. and Denness B. (1969), Observational studies on fissure patterns in cretaceous sediments of South-East England, *Géotechnique, 19, No.4.*

Fookes P.G. and Parrish D.G. (1969), Observations on small-scale structural discontinuities in the London Clay and their relationship to the regional geology. *Quart. Journal of Engineering Geol. Vol. 1, pp.217-240.*

Gens A. (1982), *Stress-strain and strength of a low plasticity clay*, PhD thesis, Imperial College of Science, Technology and Medicine, University of London.

Georgiannou V.N. (1988), *The Behaviour of Clayey Sands under Monotonic and Cyclic Loading*, PhD Thesis, University of London.

Georgiannou V.N. and Hight D.W. (1994), The effects of Centreline Tube Sampling Strains on the Undrained Behaviour of Two Stiff Overconsolidated Clays. *Geotechnical Testing Journal, GTJODJ, Vol.17, No.4, pp.475-487.*

Head, K.H. (1980), Manual of soil laboratory testing, 3Vols, London, Plymouth, Pentek.

Hight D.W. (1983), *Laboratory investigation on sea bed clays,* PhD Thesis, University of London.

Hight D.W. (2002), personal communication

Hight D.W., Jardine R.J. and Gens A. (1987), The behaviour of soft clays, *Embankments on soft clays, Public works Research Centre, Athens, Ch.2, pp.33-158.*

Hight D.J. and Jardine R.J. (1993), Small strain stiffness and strength characteristics of hard London Clay Tertiary clays. *Proc. Int. Symp. On Hard Soils-Soft Rocks, Athens, Greece, Vol. 1, pp.533-522, Balkema, Rotterdam,*

Hight D.W., McMillan F., Powell J.J.M., Jardine R.J. and Allenou C.P. (2003). Some characteristics of London Clay. *Proc. Conf. Characterisation and Engineering, National University Singapore. Tan T.S., Phoon, K.K., Hight D.W., Lerouil S. (eds). Balkema, Vol. 2, pp851-907.*

Hight D.W., Bennel J.D., Chana B., Davis P.D., Jardine R.J. and Porovic E. (1997), Wave velocity and stiffness measurements of the Crag and Lower London Tertiaries at Sizewell. *Géotechnique, 47, No.3, pp.451-474.*

Horvslev M.J. (1937), Uber die Festigkeitseirgenschaften Gestorter Bindiger Boden. Danmarks Naturvidenskabelige Samfund. *Ingeniorvidenskabelige Skrifter, A, No 45.*

Huggett J. (2005), personal communication

Huggett J.M. and Gale A.S. (1998), Petrography and diagenesis of the Thames Group at Whitecliff Bay. *Proc. Geologist Association, 109, pp.99-113.*

Jardine R.J. (1985), Investigation of pile-soil behaviour with special reference to the foundations of offshore structures. *PhD Thesis, University of London.*

Jardine R.J. (1992), Some observations on the kinematic nature of soil stiffness. *Soils and foundations, Vol.32, No. 2, pp.111-124.*

Jardine R.J. (1995), One perspective of the pre-failure deformation characteristics of some geomaterials. *Proc. of the Int. conference on the pre-failure deformation characteristics of geomaterials, Hokkaido, Japan*, Vol.2, pp. 855-885.

Jardine R.J. (2004), personal communication

Jardine R.J., Symes M.J. and Burland J.B. (1984), The measurement of soil stiffness in the triaxial apparatus, *Géotechnique, 34, No.3, pp.323-340.*

Jardine R.J., St John H.D., Hight D.W. and Potts D.M. (1991), Some practical applications of a non-linear ground model. *Proc. 10th ECSMFE, Florence, Vol.1, pp.223-228.*

Jardine R.J. and Smith P.R. (1991), Evaluation of design parameters for multi-stage construction, *Geo-coast '91 Int Conf., Yokohama, Port & Harbour Res. Ints. Yokosuka, Vol.1, pp. 197-202.*

Jardine R.J., Gens A., Hight D.W. and Coop M.R., (2004), Development in understanding Soil Behaviour. *Advances in Geotechnical Engineering: The Skempton Conference. Jardine, R.J., Potts, D.M. & Higgins, K.G. eds., Thomas Telford, London, 2003, 103-206.*

Jovicic V. and Coop M.R. (1997), Stiffness of coarse-grained soils at small strains. *Géotechnique, 47, No.3, pp.545-561.*

Jovicic V. and Coop M.R. (1998), The measurement of stiffness anisotropy in clays with bender element tests in the triaxial apparatus. *Geotechnical testing journal, GTJODJ,* Vol. 21, No1, pp.3-10.

Jovicic V., Coop M.R. and Simic, M. (1996), Objective criterial for determining Gmax from bender element tests. *Géotechnique, 46, No.2, pp.357-362.*

Kavvadas M. and Amorosi, A. (2000), A constitutive model for structured clays, *Géotechnique, 50, No.3, pp.263-273.*

King C. (1981), The stratigraphy of the London Basin and associated deposits. *Tertiary Research Special Paper*, Vol. 6, Backhuys, Rotterdam.

King C. (1991), *Stratigraphy of the London Clay (Early Eocene) in the Hampshire Basin*. PhD Thesis, Kingstone Polytechnic.

Klotz E.U., (2000). *The influence of state on the capacity of driven piles in sands*. PhD thesis, City University, London.

Kuwano R. (1999), *The stiffness and yielding anisotropy of sand.* PhD. Thesis, Imperial College of Science, Technology and Medicine, University of London

Lambe T.W. and Whitman R.V. (1969), Soil Mechanics, John Wiley & Sons Inc., New York.

La Rochelle P., Leroueil S., Trak B., Blais-Leroux L. and Tavenas F. (1988), Observational approach to membrane and area corrections in triaxial tests. *Advanced triaxial testing of soil and rock, Donaghe, Chaney Silver eds*

Leroueil S., Tavenas F. and Locat J. (1984), Discussion on: Correlations between index tests and the properties of remoulded clays- Carrier W.D. and Beckman J.F., 1984 *Géotechnique, 35, No.2, pp.223-226.*

Leroueil S. and Vaughan P. R. (1990), The General and Congruent Effects of Structure in Natural Soils and Weak Rocks. *Géotechnique, 40, No.3, pp.467-488.*

Lings M.L. (2001), Drained and undrained anisotropic elastic stiffness parameters. *Géotechnique, 51, No.6, pp.555-565.*

Lings M.L., Pennigton D.S. and Nash D.F. (2000), Anisotropic stiffness parameters and their measurement in a stiff natural clay. *Géotechnique, 50, No.2, pp.109-125.*

Love A.E.H. (1927) A treatise on the mathematical theory of elasticity. Dover publications, New York.

Lupini J.F., Skinner A.E. and Vaughan P.R. (1981), The drained residual strength of cohesive soils. *Géotechnique, 31, No.2, pp.181-213.*

Ma J.D.H (2003), *Behaviour of intact London Clay in oedometer tests.* MSc dissertation, Imperial College London.

Maguire W.M. (1975), *The undrained strength and stress-strain behaviour of brecciated Upper Lias clay.* PhD Thesis, University of London.

Mannion W. (2004), *Stratigraphical studies relevant to the geotechnics of the London Basin. MPhil transfer report*, Imperial College London.

Marsland A. (1971), The shear strength of stiff fissured clays. *Stress-strains behaviour of soils, Roscoe Memorial Symposium, pp.59-68. Cambridge: G.T. Foulis.*

Marsland A. and Butler M.E. (1967), Strength measurements on stiff fissured Barton Clay from Hampshire. *Proc. Geotech. Conf. Oslo 1, pp.139-145.*

Mayne P.W. and Kulhawy F.H. (1982), K_o-OCR relationship in soil. *ASCE, GT6, Vol.108, pp.851-872.*

Mitchell J.K. (1960) Fundamental aspects of thixotropy in soils. *Journal of SMFE Div., Proc of ASCE, 83 No3, pp.19-52.*

Momoya Y. (1998), *Effects of the period and stress path of consolidation on consolidation characteristics of clays.* MSc Thesis, University of Tokyo (in Japanese).

Momoya Y. Ishii T. and Tatsuoka F. (1998), Strain-rate dependency of deformation on NC clay and prediction of undrained creep. *Proc. 33rd Japan National Conference on Geotechnical Engineering, JGS, Yamaguchi 1, pp.615-616 (in Japanese).*

Nishimura S. (2005), *Laboratory study on anisotropy of natural London Clay.* PhD thesis to be submitted to Imperial College London.

O'Brien N.R. and Slatt R.M. (1990), Argillaceous Rock atlas, Springer Velag.

Pennington D.S., Nash D.F.T. and Lings M.L. (1997), Anisotropy of Go shear stiffness in Gault clay. *Géotechnique, 47, No.3, pp.391-398.*

Pickering D.J. (1970), Anisotropic elastic parameters for soils. *Géotechnique, 20, No.3, pp.271-276.*

Porovic E. and Jardine R.J. (1995), Some observations on the static and dynamic shear stiffness of Ham River sand. *Pre-failure deformation of geomaterials, Balkema, Rotterdam*, Vol.1, pp.25-30.

Pun A. (2003), *The influence of structure on the compression behaviour of London Clay.* MSc dissertation, Imperial College London.

Puzrin A.M. and Burland J.B. (1998), Non-linear model of small-strain behaviour of soils, *Géotechnique, 20, No.4, pp.217-233.*

Qadimi A., (2005), *The cyclic response of a carbonate sand through critical state soil mechanics.* PhD Thesis, Imperial College London.

Rampello S. (1989), *Effetti del rigonfiamento sul compartamento di argille fortemente sovraconsolidate.* PhD Thesis, University of Rome.

Richardson D. (1998), *Investigation of threshold effects in soil deformations.* PhD Thesis, City University, London.

Ridley A.M. and Burland J.B. (1993), A new instrumentation for the measurement of soil moisture suction. *Géotechnique, 43, No.2, pp.321-324.*

Rolo R. (2003), *The anisotropic stress-strain-strength behaviour of brittle sediments.* PhD Thesis, Imperial College of Science, Technology and Medicine, London.

Sandroni S. (1977), *The strength of London Clay in total and effective stress terms,* PhD Thesis, University of London

Santucci de Magistris F. (1998), *Internal report,* Geotechnical Engineering Laboratory, University of Tokyo

Schmertmann, J.H. (1969), Swell Sensitivity. *Géotechnique, 19, No.41, pp.530-533.*

Sides G. and Barden L. (1970), The microstructure of dispersed and flocculated samples of kaolinite, illite and montmorillonite, *Canadian Geotechnical Journal, 8, pp.391-399.*

Simpson B. (1992), Retaining Structures: displacement and design. *Géotechnique, 42, No.4, pp.541-576.*

Simpson B., O'Riordan N.J. and Croft O.D. (1979), A computer model for the analysis of ground movements in London Clay. *Géotechnique, 29, No.2, pp.149-175.*

Simpson B., Calabresi G., Sommer H. and Wallays (1981), Design parameters for stiff clays. *State of the art report, Session 4, Proc.7th European Conf. on Soil Mech Geoth. Eng., Brighton 5, pp.91-125.*

Simpson B., Atkinson J.H. and Jovicic V. (1996), The influence of anisotropy on calculations of ground settlements above tunnels. *Proceedings, Geothecnical Aspects of underground construction in soft ground, Balkema, Rotterdam, pp.591-595.*

Skempton A.W. (1944), Notes on the compressibility of clays. *Q.J. Geological Soc. No.100, pp.119-135.*

Skempton A.W. (1961), Horizontal stresses in an overconsolidated Eocene clay, Proc. 5th ICSMFE, Paris 1, pp.351-357.

Skempton A.W. (1964), Long term stability of clay slopes. *Géotechnique, 14, No.2, pp.77-101.*

Skempton (1970), The consolidation of clays by gravitational compaction. *Q.J. Geological Soc. No.125, pp373-411.*

Skempton A.W. (1977), Slope stability of cutting in brown London Clay. *Proc.9th Int. Conf. Soil Mech. and Fund. Eng., Tokyo, 3, pp.261-270.*

Skempton A.W. and La Rochelle P. (1965), The Bradwell slip: a short-term failure in London Clay. *Géotechnique, 15, No.3, pp.221-242.*

Skempton A.W. and Henkel D.J. (1957), Tests on London Clay from deep borings at Paddington, Victoria and the South Bank. *Proc. 4th Int. Conf. S.M. & F.E., London, 1, pp. 100-106.*

Skempton A.W. and Northey R.D. (1952), The sensitivity of clays. *Géotechnique, 3, No.1, pp.30-53.*

Skempton A.W. and Petley D.J. (1967), The strength along structural discontinuities in stiff clays. *Proc. Geotech. Conf., Oslo, 2, pp.29-46.*

Skempton A.W., Schuster F.R.S. and Petley D.J. (1969), Joints and fissures in the London Clay at Wraysbury and Edgware, *Géotechnique, 19, No.2, pp.205-217*

Shirley D.J. and Hampton L.D. (1997), Shear Wave Measurements in Laboratory Sediments. *Journal of Acoustic Society of America, Vol.63, No3, pp.607-613.*

Smart P. and Tovey N.K., (1982), Electron microscopy of soils and sediments: examples, *Oxford University Press, p.178.*

Smith P.R. and Jardine R.J. (1991), The use of triaxial tests for prediction of settlements. *Geo-Coast '91, Yokohama, Vol.1/17, pp.89-91.*

Smith P., Jardine R.J. and Hight D.W. (1992), The yielding of Bothkennar clay, *Géotechnique, 42, No.2, pp.257-274*

Som N.N. (1968), *The effects of stress path on deformation and consolidation of London Clay.* PhD Thesis, University of London

Stallebrass S.E. and Taylor R.N. (1997) The development and evaluation of a constitutive model for the prediction of ground movements in overconsolidated clay, *Géotechnique, 47, No.2, pp.235-353.*

Standing J.R. and Burland J.B. (1999), Ground characterisation to explain JLEP Tunnelling Volume Losses in the Westminster area. *Report to LUL.*

Standing J.R. and Burland J.B. (2005a), Investigationg variations in tunnelling volume loss –a case study. *Proc. Int. Conf. Geotechnical Aspects of Underground Construction in Soft ground, Amsterdam, Balkema, in print*

Standing J.R. and Burland J.B. (2005b), An investigation into unexpected tunnelling volume losses in the Westminster area, London, *submitted to Géotechnique*

Takahashi A. Jardine R.J. and Dennis W.H. (2005), Swelling effects on mechanical behaviour of natural London Clay. *Proc. 16th Int. Conf. Soil Mech., Osaka, in print.*

Tatsouka F., Santucci de Magistris F., Hayano K., Momoya Y. and Koseki J. (1998), Some new aspects of time effects on the stress-strain behaviour of stiff geomaterials. *2HSSR, Napoli, 1998.*

Terzaghi K. (1944), Ends and means in Soils Mechanics, *Engineering Journal (Canada), Vol.27, p.608.*

Vaughan P.R. (1997), Engineering behaviour of weak rock: Some answers and some questions. *Proc. Of the First Int. Conf. On Hard Soils and Soft Rocks, 3, pp.1741-1765. Rottherdam: Balkema.*

Vaughan P.R., Hight D.W., Sodha V.G. and Walbanke H.J. (1978), Factors controlling the stability of clays fills in Britain. *Clay Fills, Institution of Civil Engineers, London, pp.203-217.*

Veniale, F. (1985), The role of microfabric in clay soil stability, *Miner. Petrogr. Acta, Vol. 29-A, pp.101-119.*

Viggiani G. and Atkinson J.H. (1995), Interpretation of bender element tests, *Géotechnique, 45, No.1, pp.149-154.*

Viladesau E. (2003), *Effects of swelling on the strength of London Clay,* Imperial College London, internal report.

Walsh J.B. (1965), The effects of cracks on the uniaxial elastic compression of rocks. *J. Geotech. Res. 70, pp.5249-5257.*

Ward W.H., Marsland A. and Samuels S.G. (1965), Proprieties of the London Clay at the Ashford Common shaft: in-situ and undrained strength tests *Géotechnique 15, No.4, pp.321-344.*

Ward W.H., Samuels S.G. and Butler, M.E. (1959), Further studies of the proprieties of London Clay *Géotechnique, 9, No.2, pp.33-58.*

Webb D. L. (1964), *The mechanical proprieties of undisturbed samples of London Clay and Pierre shale.* PhD. Thesis, University of London.

Wroth C.P. (1972), Some aspects of the elastic behaviour of overconsolidated clay. *Proc. Roscoe Memorial Symp., Foulis, pp.347-361.*

Wongsaroj J., Soga K., Yimsiri S. and Mair R.J. (2004), Stiffness anisotropy of London Clay and its modelling: Laboratory and Field. *Advances in Geotechnical Engineering: The Skempton Conference, 2004, Thomas Telford, London.*

Yimsiri S. (2001), *Pre-failure deformation characteristics of soils: Anisotropy and soil fabric*. PhD Thesis, University of Cambridge.

APPENDIX 5.1

Calculation of the in situ stress states and approach stress paths

For the samples that were consolidated to the in situ stress states, four representative depths were chosen; "35m" for samples from 34 to 40m, "25m" for samples from 22 to 32.5m, "10m" for samples from 10 to 12.5m and "7m" for the block samples from the top of the London Clay. For these representative depths the in situ stresses p' and q were calculated considering the geometry of the site, sketched in Figure A5.1 and the k_o profile suggested by Hight et al., (2003) (Figure A5.2), which was derived from the suction measurements on thin-walled samples (see Section 3.5.3). About 5.5m of gravel was assumed to overlay about 52m of London Clay. The site investigation showed that the water table was 1.5m above the top of the clay and the pore water pressure was found to be hydrostatic. Table A5.1 shows the stresses used. For samples from "10m" and "7m" the same in situ stress point was used as discussed in Section 5.3.5.

The geological stress history of the London Clay at the site was simulated for each representative depth, the same stress history being assumed for samples from 10 and 7m depths. Three geological phases were supposed: the deposition of clay, the erosion of clay and the deposition of gravel. It was assumed that about 175m of the upper part of the clay above the present level have been eroded at this location (Skempton & Henkel, 1957; Chandler, 2000). The OCR values are shown in Table A5.1. Figure A5.3 sketches the geological stress paths for the three depths. The values of k_o used were:

$$\textit{Phase I:} \quad k_o = 1 - \sin\varphi' \tag{A5.1}$$

$$\textit{Phase II:} \quad k_o = \left(1 - \sin\varphi'\right) OCR^{\sin\varphi'} \tag{A5.2}$$

$$\textit{Phase III:} \quad k_o = k_{oNC}\left[\frac{OCR}{OCR_{max}^{1-\sin\varphi'}} + \frac{3}{4}\left(1 - \frac{OCR}{OCR_{max}}\right)\right] \tag{A5.3}$$

as suggested by Mayne & Kulhawy (1982), where OCR is the overconsolidation ratio. Table A5.2 shows the details of the geological stress paths.

The final in situ stresses derived from the geological stress history were different from those calculated using the geometry of the site and the k_o values suggested by Hight et al. (2003). This difference might arise from the fact that the simulation of the geological stress path was very simplistic. Taking into consideration the influence of the sea level changes during the depositional process and the presence of the lithological units, it is likely that several cycles of deposition and erosion occurred in the London Clay at different stages of its geological life (Chandler, 2002), before the final deposition of the gravel. The development of bonding during the geological history of the clay was also neglected. These factors might have caused changes of k_o and moved the in situ stress point.

Considering the difficulty in simulating a more complex geological history of the clay, the simplified "three phase" geological stress path was assumed to be valid, but it was shifted, keeping the stress paths parallel, in order to match the measured in situ stress points (Figure A5.4). The re-loading stress path due to the deposition of the gravel is likely to reproduce quite realistically the last geological event on this site and it is expected to have a more significant influence on the sample behaviour, therefore the simplified assumption made by shifting the geological stress paths was considered adequate. Two stress path approaches were used, in agreement with the research group involved in the London Clay project.

Long geological stress path

This approach stress path is illustrated in Figure A5.5a. It consisted of isotropic compression to a maximum effective stress determined at the intersection of the geological unloading line with the isotropic axis (A to B), unloading along the k_o line (B to C) and reloading to the in situ stress point (C to O). Table A5.2 shows the stresses used for the approach stress paths for each depth. This approach stress path was performed only on two samples from

"35m" depth (Tests 36lgUC, 38.7lgUC), because large volumetric strains of about 2% developed during the isotropic compression. These large strains might induce excessive disturbance to the sample structure, and therefore a second stress path was chosen for all the other tests.

Short geological stress path

This approach stress path, illustrated in Figure A5.5b, consisted of isotropic compression to the mean effective stress corresponding to the in situ stress (A to B'), unloading at constant p' to reach the stress point on the geological unloading curve (B' to C'), and then unloading and reloading along the geological stress path to the in situ point (C' to C and C to O). Maximum limits of 1% volumetric strain and 0.5% axial strain were imposed for this second approach stress path. Only in a few cases were these limits slightly exceeded.

10 and 7m depths

An atypical stress path was followed by the samples from "10m" and "7m" depth, because the calculated in situ stress points could not be reached as failures in extension would occur. Initial tests attempted on samples from 10m depth showed that the fixed limits of 0.5% axial strain and 1% volumetric strain imposed for the "short geological stress path" could not be respected and one sample also failed on a pre-existing fissure before reaching the in situ stress state. It was therefore decided to stop the approach stress path at a stress point along the constant p' unloading, which could safely be reached by all the samples from 7m and 10m depths without exceeding the strain limits. This stress point corresponded to p'=260kPa and q=-86kPa and was assumed to be the new representative in situ stress point for samples from this depth. The modified stress path for these depths is shown in Figure A5.5c.

Special cases

Test 24g37DC

In this test, the sample, from 24m depth, was consolidated along the "25m" stress path to its reference in situ stress state. From this point, after performing probes, the sample was re-consolidated to the "37m" in situ state following the

stress path sketched in Figure A5.5d. Probes were again performed at this point before shearing the sample to failure.

Test 31.4gUE

The sample used for this test was from 31.4m depth. Although it belongs to Unit B_2, it was consolidated to the "35m" depth stress point by following the "35m" approach stress path because, at the time of testing, the division into lithologcial units was not yet clear and this sample was believed to belong Unit A_3.

Test 25.4aUE

This test was supposed to follow a long approach stress path to the in situ stress state of the reference depth "25m", but a computer crash occurred during the test, which changed the calibration factor of the load cell. The final stress state did not coincide therefore with the expected state. For this reason the letter "a" in the name of this sample indicates an anisotropic stress condition of p'=440kPa and q=-20kPa.

Test 11.9DE

This test was performed in a earlier stage of the research, when the in situ effective stress of p'=260kPa and q=–220kPa was supposed to be reached following the stress path for "10m" depth. The sample, though, failed prematurely along a pre-existing fissure during the constant p' stage. After this test the stress path for "7m" and "10m" was modified as described above.

Depth from ground level	Thickness of gravel	Depth from top of LC	k_o	γ_{clay}	σ'_v	OCR	p'	q
[m]	[m]	[m]		kN/m^3	[kPa]		[kPa]	[kPa]
7	5	1	3	21	111	16.0	258	-222
25		20	1.5		309	6.5	413	-157
36		30	1.3		426	5.0	508	-124

Table A5.1: Tests from the in situ stress point: in situ stresses

Unit	Sample name	Reference depth	In situ stresses p' [kPa]	In situ stresses q [kPa]	Approach stress path	
C	7gUC 7gUE 7kUC	"7m"	260	-220	A - B' - O' (Figure A5.5(c))	B' (p'=260kPa ; q=0kPa) O' (p'=260kPa ; q=-86kPa)
B_2	11gUC 11gkUC 11gDE 12.5gUC	"10m"				
B_2	22gsUC 22.6gUC 23gUE 24g37DC 24.3gkUC 24.4gsUC 25gUC	"25m"	420	-155	A - B' - C' - C - O (Figure A5.5(b))	B (p'=820kPa ; q=0kPa) B' (p'=420kPa ; q=0kPa) C' (p'=420kPa ; q=-195kPa) C (p'=365kPa ; q=-209kPa)
A_3	31.4gUE 33.5gkUC 36.3g 36.3gUE 36.5gDC	"35m"	510	-125	A - B' - C' - C - O (Figure A5.5(b))	B (p'=820kPa ; q=0kPa) B' (p'=420kPa ; q=0kPa) C' (p'=420kPa ; q=-195kPa) C (p'=365kPa ; q=-209kPa)
	36lgUC 38.7lgUC		510	-125	A - B - C - O (Figure A5.5(a))	

Table A5.2: In situ stresses and approach stress paths (refer to Figure 5.5)

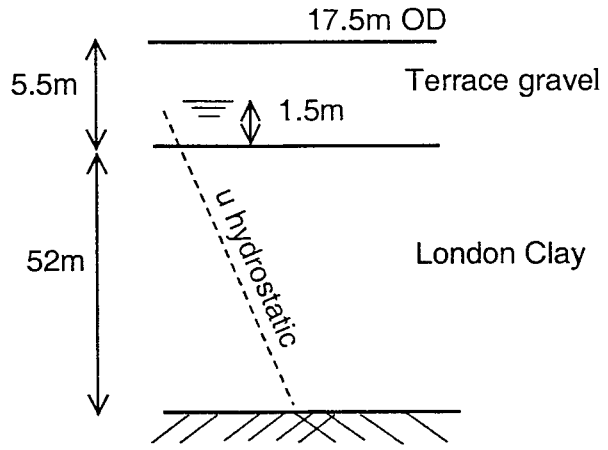

Figure A5.1: Sketch of the geometry of the site

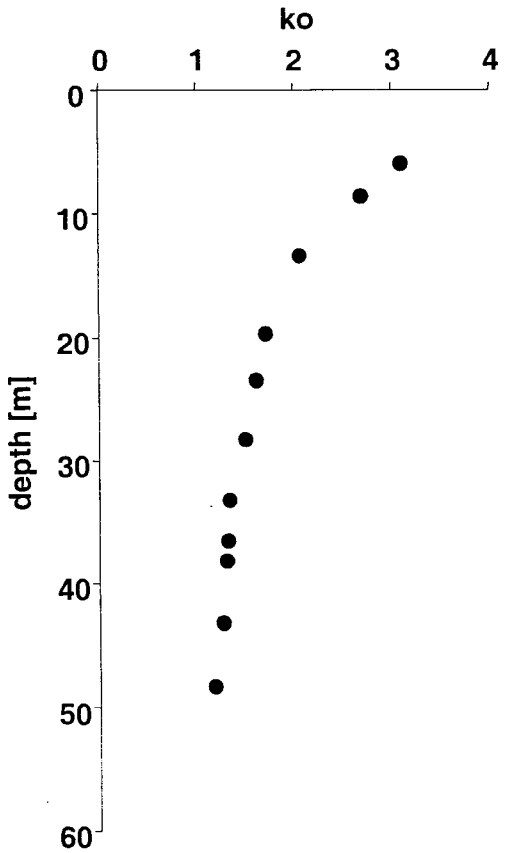

Figure A5.2: k_o profile derived from suction measurements on thin-walled samples (Hight et al. 2003)

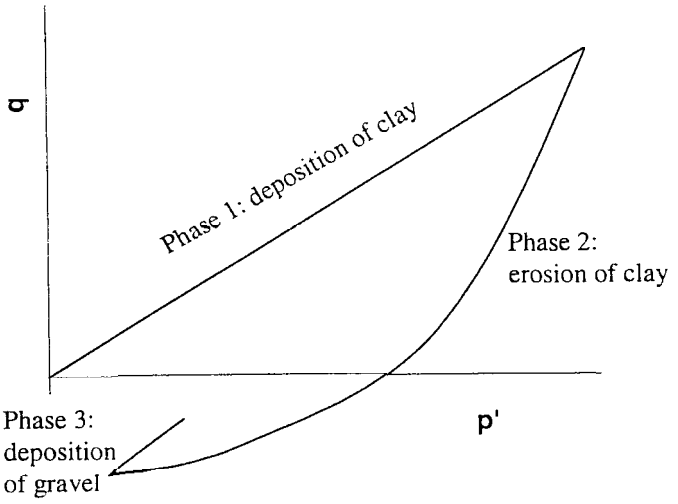

Figure A5.3: Schematic geological stress history of London Clay at T5

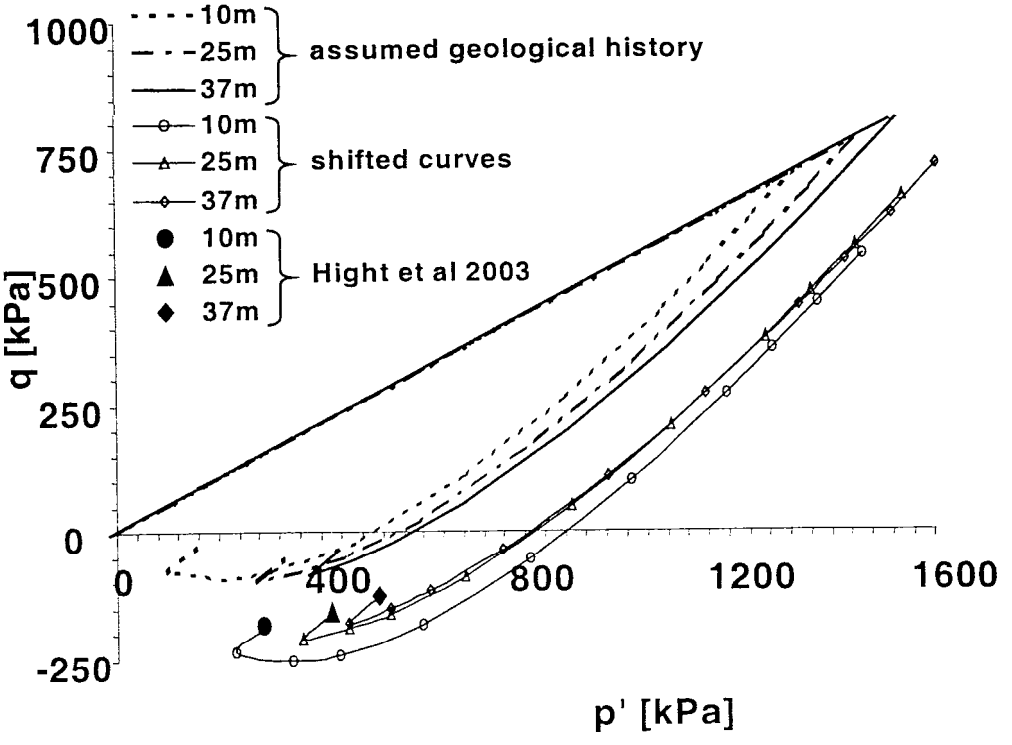

Figure A5.4: Estimated geological stress paths, shifted stress paths and in situ stress points for the three reference depths

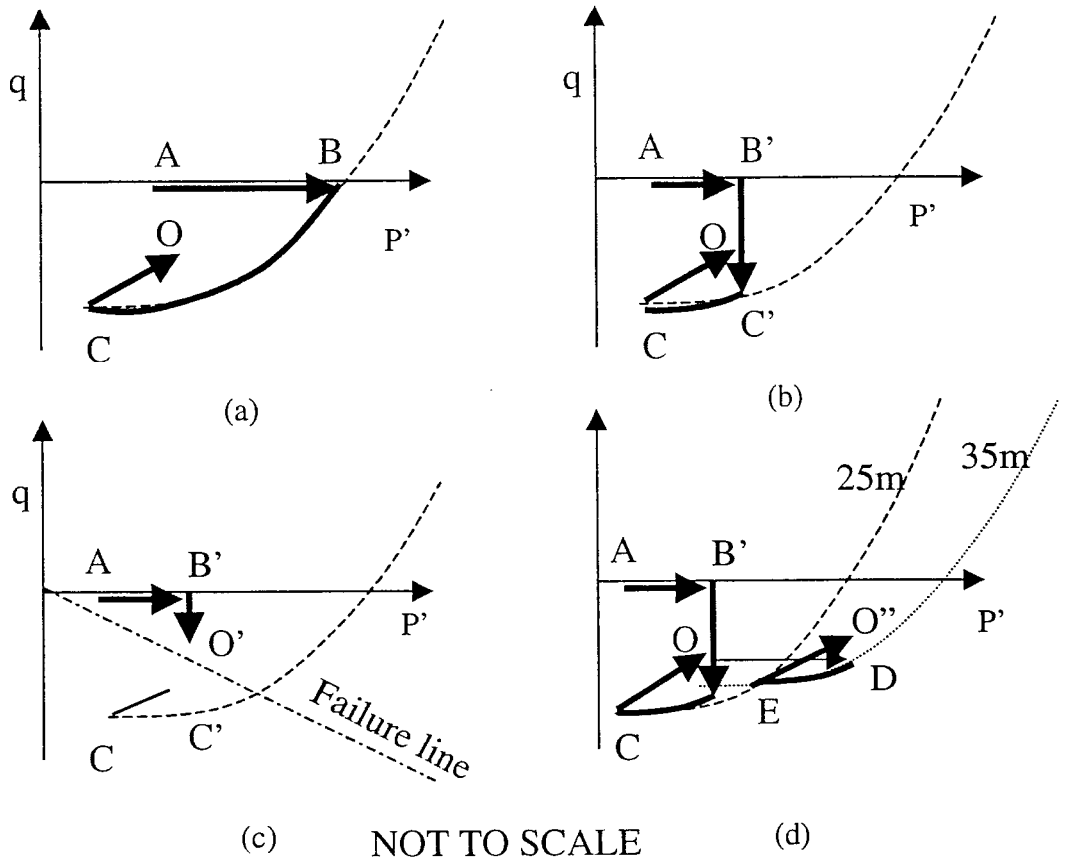

Figure A5.5: Approach stress paths to the in situ stress states (a) long path for "25m" and "37m" depths ((b) short path for "25m" and "37m" depths (c) path for "7m" and "10m" depths (d) path of Test 24g37DC

APPENDIX 5.2

Measurements of the elastic parameters

The elastic parameters of the clay were measured by performing bender element tests and small stress controlled drained probes following the analysis described in Section 2.4.

The set of bender elements mounted on the samples allowed the measurements of the shear moduli G_{hh} and G_{hv}, which were calculated using Equations 2.21 and 2.22. For these equations, the arrival time was determined interpreting the bender element signal with both the "first arrival method" and the "frequency method", as described in Section 2.5.1. Figures A5.6 and 5.7 show two examples of the interpretation methods. Sinusoidal waves were used with frequencies in the range 2-12kHz. Usually a clear signal was obtained, as shown, for example, in Figure A5.6. The two interpretation methods always gave values in good agreement. The arrival time determined with the first arrival method could be influenced by near field effects, so that it decreased slightly with increasing frequency, as shown in Figure A5.8, where the arrival times determined by the two methods are shown for different frequencies. The arrival time determined with the frequency method usually coincided with the values determined with the first arrival method using higher frequencies and was used in Equations 2.21 and 2.22 for the calculation of the shear moduli. A detailed analysis of the interpretations at the different depths will be given in Chapter 8.

The drained probes were chosen so that the elastic parameters could be measured from the equations:

$$\delta\varepsilon_a = \frac{1}{E_v}\delta\sigma'_a - \frac{2\nu_{vh}}{E_v}\delta\sigma'_r \qquad \text{(A5.4)}$$

$$\delta\varepsilon_r = -\frac{\nu_{vh}}{E_v}\delta\sigma'_a + \frac{1-\nu_{hh}}{E_h}\delta\sigma_r \qquad \text{(A5.5)}$$

For axial compression or extension, $\delta\sigma_r'=0$ reducing the equations (A5.4) and (A5.5) to:

$$\delta\varepsilon_a = \frac{1}{E_v}\delta\sigma'_a \qquad \text{(A5.6)}$$

$$\delta\varepsilon_r = -\frac{\nu_{vh}}{E_v}\delta\sigma'_a \qquad \text{(A5.7)}$$

The vertical Young modulus E_v in compression or extension and the Poisson's ratio ν_{vh} were directly measured from Equations A5.6 and A5.7:

$$E_v = \left(\frac{\delta\sigma'_a}{\delta\varepsilon_a}\right)_{\delta\sigma'_r=0} \qquad \text{(A5.8)}$$

$$\nu_{vh} = \left(\frac{\delta\varepsilon_r}{\delta\varepsilon_a}\right)_{\delta\sigma'_r=0} \qquad \text{(A5.9)}$$

For radial compression, $\delta\sigma_a'=0$, reducing Equations 5.4 and A5.5 to:

$$\delta\varepsilon_a = -\frac{2\nu_{vh}}{E_v}\delta\sigma'_r \qquad \text{(A5.10)}$$

$$\delta\varepsilon_r = \frac{1-\nu_{hh}}{E_h}\delta\sigma_r \qquad \text{(A5.11)}$$

and so the horizontal Young's modulus E_h and the other Poisson's ratios ν_{hh} and ν_{vh} were derived following Kuwano (1999) and the three parameters formulation suggested by Lings et. al. (2000). A parameter F was directly measured from the probes, where:

$$F_h = \frac{E_h}{1-\nu_{hh}} \qquad \text{(A5.12)}$$

Having measured the shear modulus G_{hh} using the bender elements, the horizontal Young's Modulus was calculated from:

$$E_h = \frac{4F_h G_{hh}}{F_h + 2G_{hh}} \qquad \text{(A5.13)}$$

The Poisson's ratio ν_{hh} was calculated from the combination of Equations A5.12 and A5.13, and ν_{vh} was calculated using the average value from the equations:

$$\nu_{hv} = -\frac{\delta\varepsilon_a}{\delta\varepsilon_r}\frac{(1-\nu_{hh})}{2} \qquad \text{(A5.14)}$$

$$\nu_{hv} = -\frac{E_h}{2}\frac{\delta\varepsilon_a}{\delta\sigma_r} \qquad \text{(A5.15)}$$

Probes at constant p' and constant q were also performed. These probes allowed measurements of the bulk modulus K, the equivalent shear modulus G_{eq} and the coupling moduli J_{pq} and J_{qp}, from the constitutive equations written in terms of triaxial variables (Atkinson et al., 1990):

$$\delta\varepsilon_v = \frac{\delta p'}{K} + \frac{\delta q}{J_{pq}} \qquad \text{(A5.16)}$$

$$\delta\varepsilon_s = \frac{\delta p'}{J_{pq}} + \frac{\delta q}{3G_{eq}} \qquad \text{(A5.17)}$$

For an elastic material the compliance matrix has to be symmetrical, therefore J_{pq}=J_{qp},=J. The parameters measured from the constant p' and constant q probes, from Equations A5.16 and A5.17, were then compared with those calculated by using the other elastic parameters derived from the constant σ'_r and σ'_a probes and bender elements:

$$G_{eq} = \frac{3}{4\left[(1+2\nu_{vh})/E_v + (1-\nu_{hh})/2E_h\right]} \qquad \text{(A5.18)}$$

$$K = \frac{1}{\left[(1-4\nu_{vh})/E_v + 2(1-\nu_{hh})/E_h\right]} \qquad \text{(A5.19)}$$

$$J = \frac{3}{2[(1-\nu_{vh})/E_v - (1-\nu_{hh})/E_h]} \tag{A5.20}$$

This comparison enabled a check to be made of consistency of the elastic parameters.

The undrained parameters were also calculated as combination of the drained parameters using the formulation proposed by Lings (2001). As discussed in Section 2.5.1, the mapping is only possible from drained to undraned parameters and the calculated values were compared with the values measured directly from undrained tests. For undrained conditions, ν_{vh}=0.5 and the other undrained elastic parameters can be derived from:

$$E_v^u = \frac{E_v[2(1-\nu_{hh})E_v + (1-4\nu_{vh})E_h]}{2(1-\nu_{hh})E_v - 4\nu_{vh}^2 E_h} \tag{A5.21}$$

$$E_h^u = \frac{E_h[2(1-\nu_{hh})E_v^2 + (1-4\nu_{vh})E_v E_h]}{(1-\nu_{hh}^2)E_v^2 + (1-2\nu_{vh}-2\nu_{vh}\nu_{hh})E_v E_h - \nu_{vh}^2 E_h^2} \tag{A5.22}$$

$$\nu_{hh}^u = \frac{(1-\nu_{hh}^2)E_v^2 + (\nu_{hh}-2\nu_{vh}-2\nu_{vh}\nu_{hh})E_v E_h + \nu_{vh}^2 E_h^2}{(1-\nu_{hh}^2)E_v^2 + (1-2\nu_{vh}-2\nu_{vh}\nu_{hh})E_v E_h - \nu_{vh}^2 E_h^2} \tag{A5.23}$$

$$\nu_{hv}^u = \frac{\nu_{vh}^u E_h^u}{E_v^u} \tag{A5.24}$$

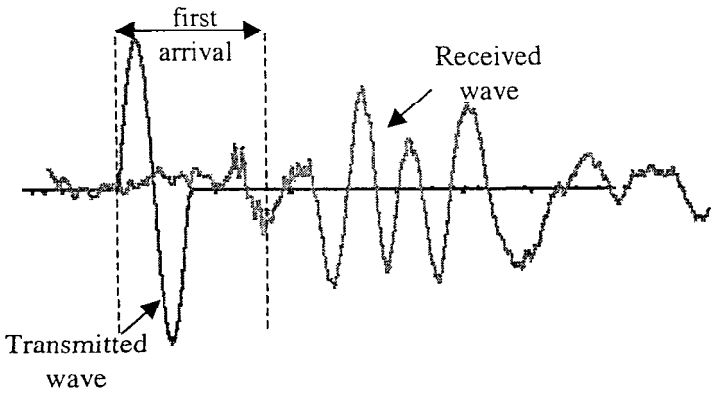

Figure A5.6: Shear wave signal and first arrival time

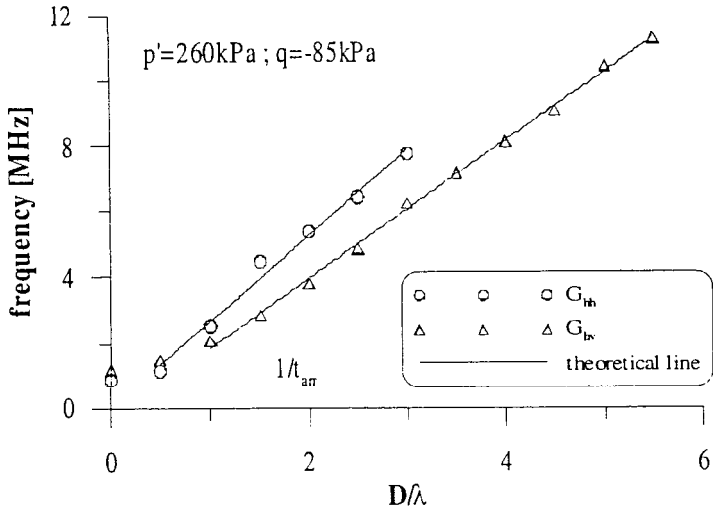

Figure A5.7: Arrival time determined with the frequency method

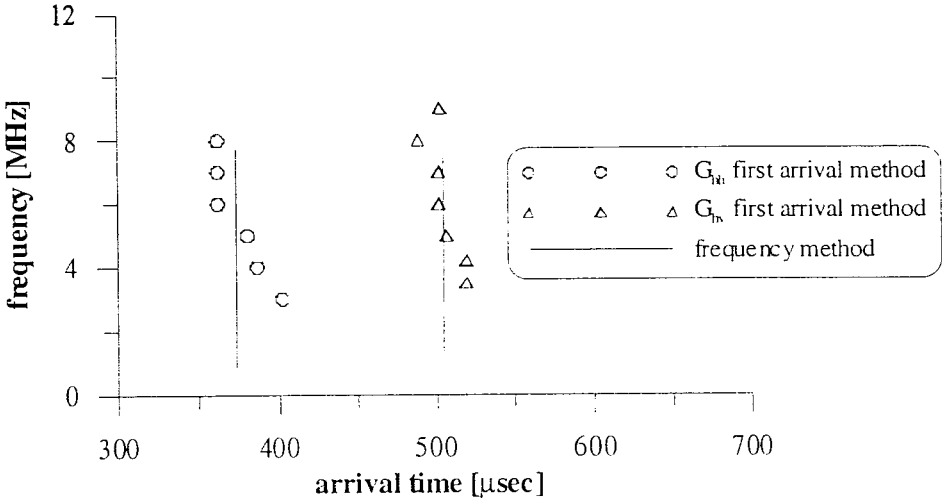

Figure A5.8: Comparison between the arrival times determined with the first arrival and the frequency method

APPENDIX 7.1

Shear planes

The figures in this appendix show schematic drawings of the shear planes formed in samples from different lithological units.

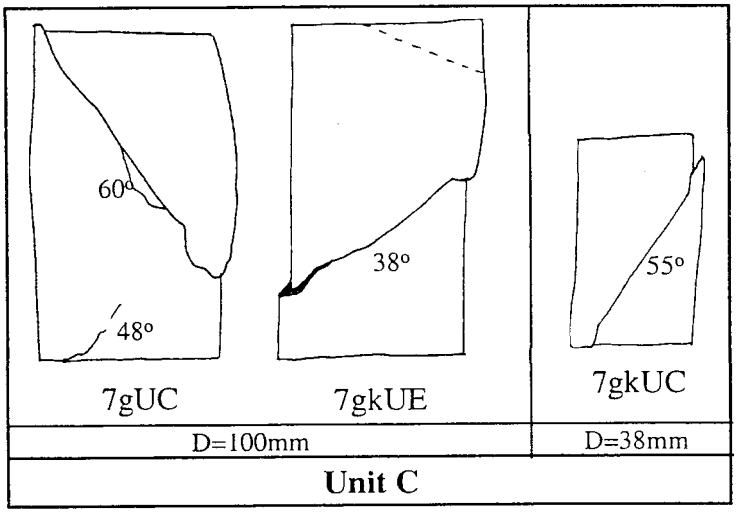

Figure A7.1: Shear plane characteristics for samples from Unit C

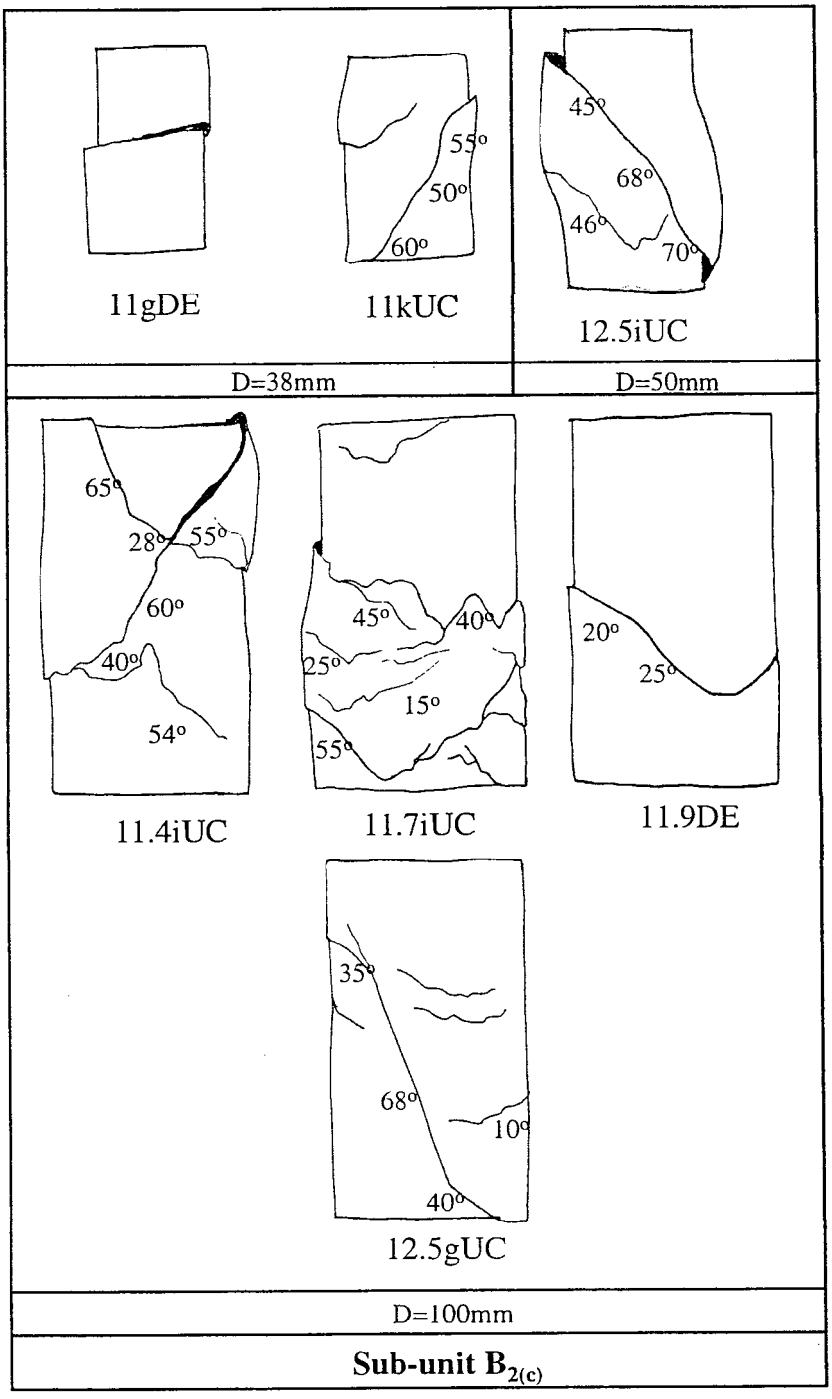

Figure A7.2: Shear plane characteristics for samples from Sub-Unit $B_{2(c)}$

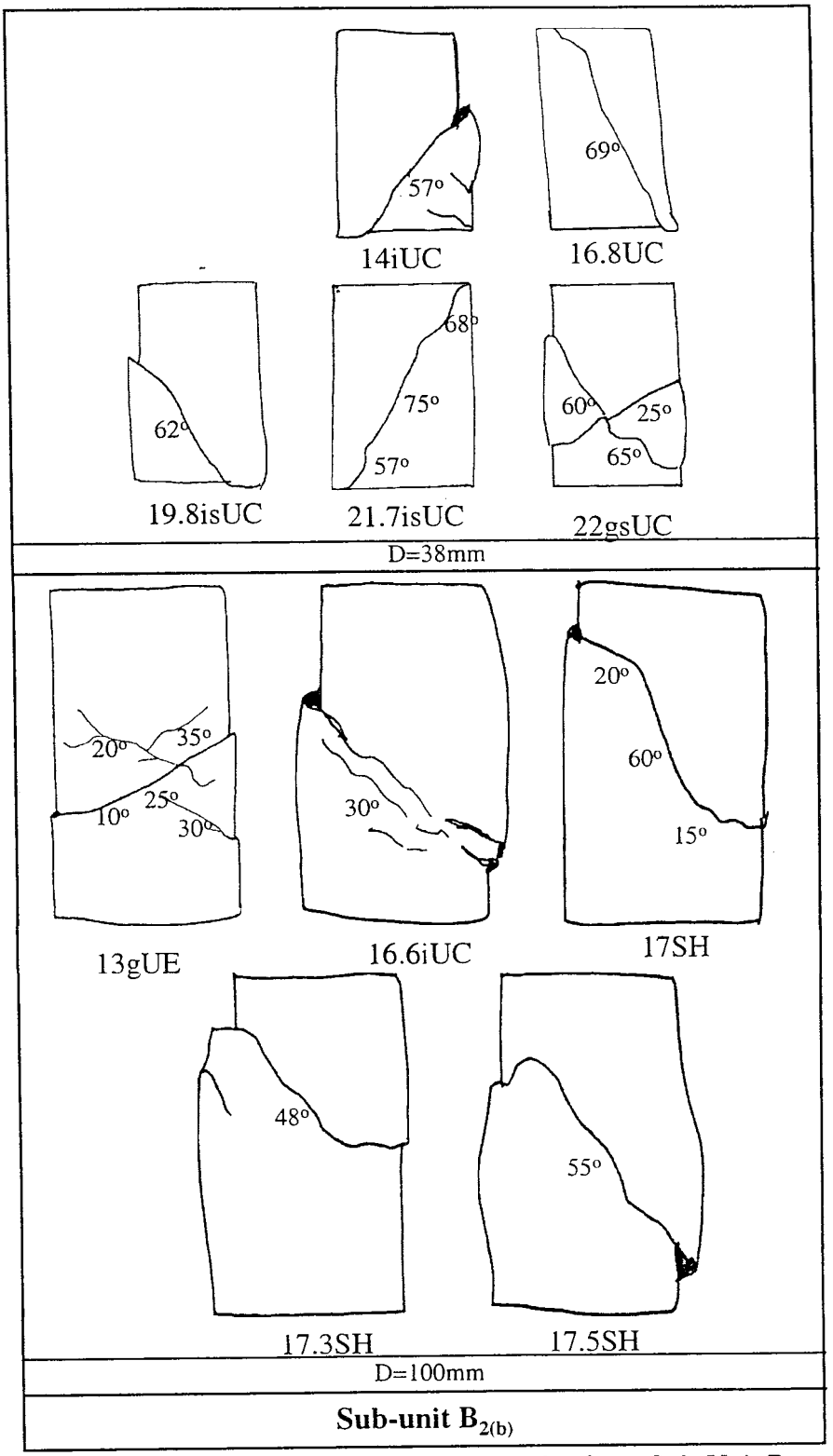

Figure A7.3: Shear plane characteristics for samples from Sub-Unit $B_{2(b)}$

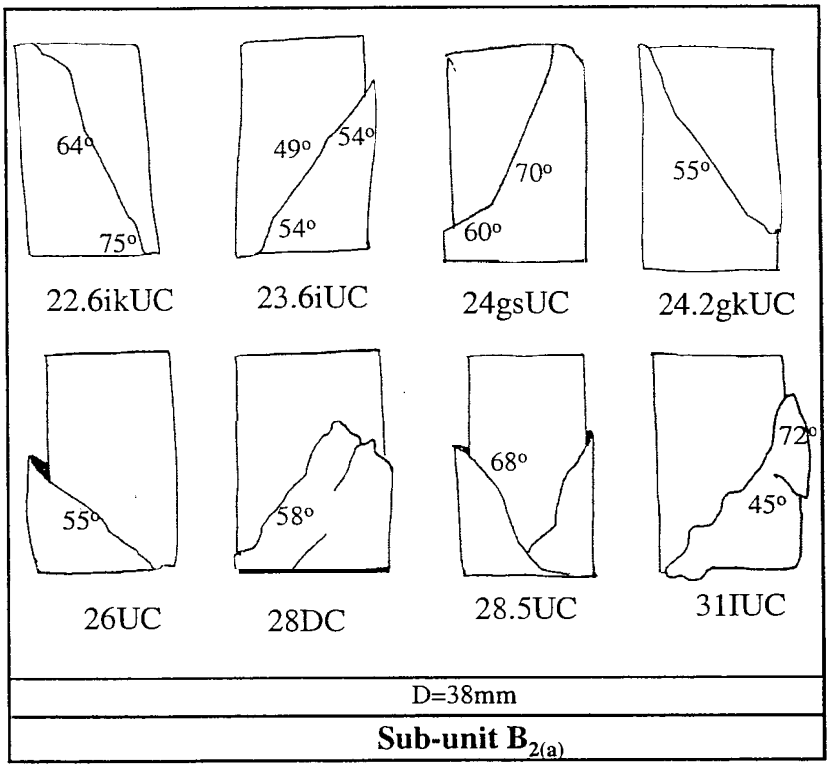

Figure A7.4: Shear plane characteristics for 38mm diameter samples from Sub-Unit $B_{2(a)}$

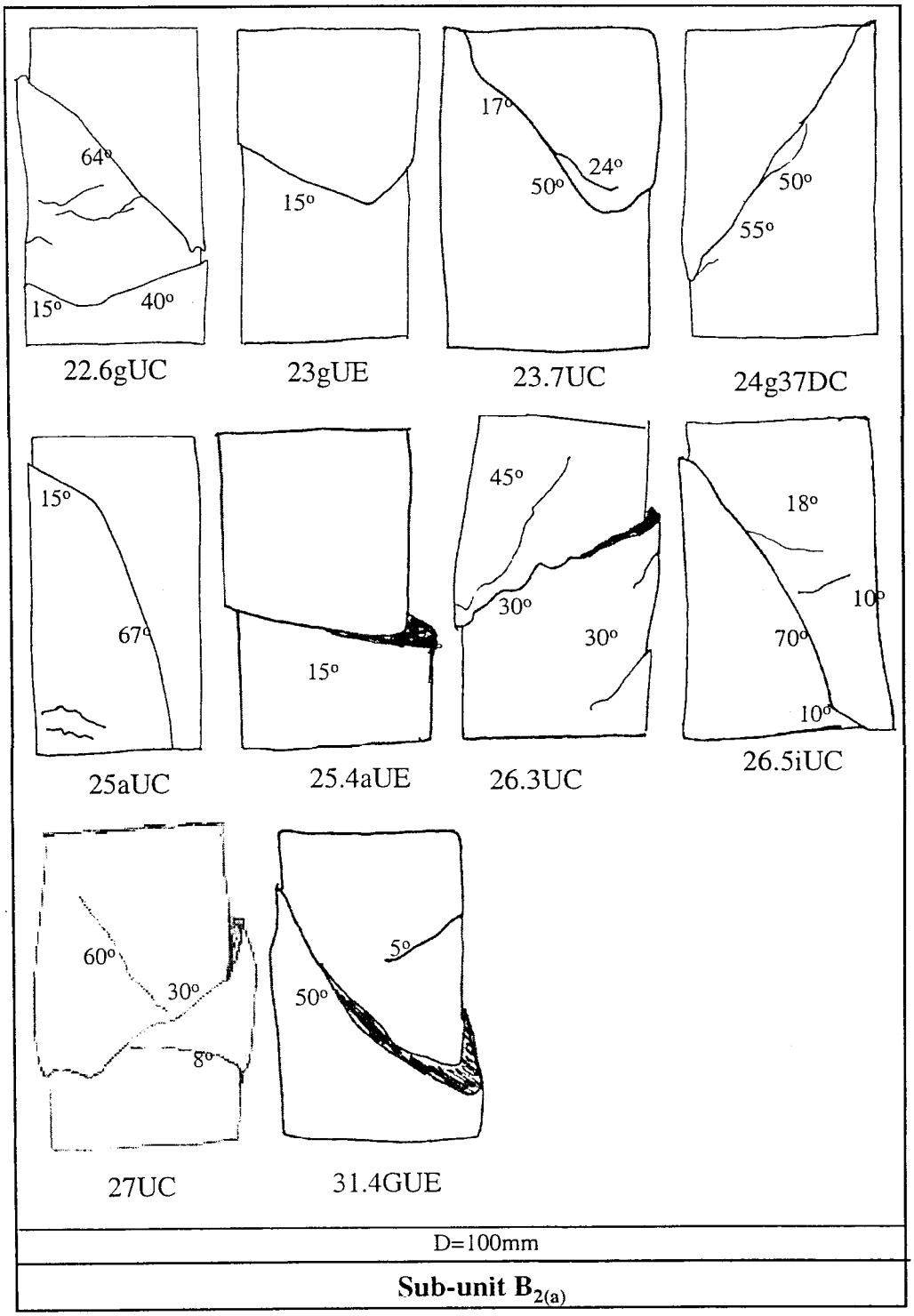

Figure A7.5: Shear plane characteristics for 100mm diameter samples from Sub-Unit $B_{2(a)}$

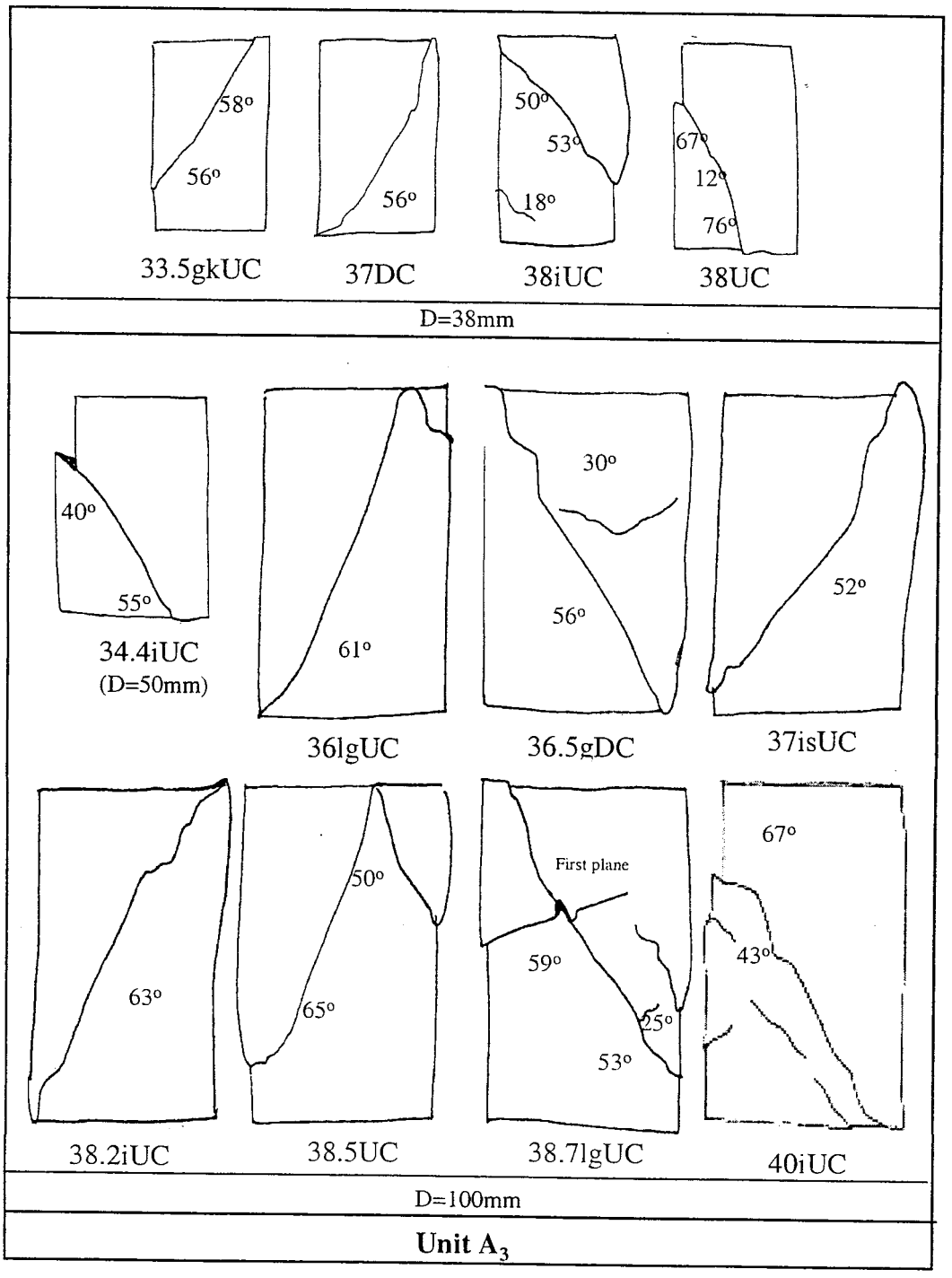

Figure A7.6: Shear plane characteristics for samples from Unit A_3